

长江中下游贵池李湾铜多金属矿区岩浆岩年代学及 Hf 同位素地球化学研究^{*}

段留安^{1,2} 古黄玲¹ 杨晓勇^{1**} 严志忠³ 孙卫东^{4,5}

DUAN LiuAn^{1,2}, GU HuangLing¹, YANG XiaoYong^{1**}, YAN ZhiZhong³ and SUN WeiDong^{4,5}

1. 中国科学技术大学地球和空间科学学院, 合肥 230026

2. 武警黄金第七支队, 烟台 264004

3. 安徽省地勘局 324 地质队, 池州 247100

4. 中国科学院广州地球化学研究所矿物学与成矿学重点实验室, 广州 510640

5. 中国科学院青藏高原地球科学卓越创新中心, 北京 100101

1. School of Earth and Space Sciences, University of Science and Technology of China, Hefei 230026, China

2. The 7th Gold Detachment of Chinese People's Armed Police Force, Yantai 264004, China

3. The 324 Geological Team, Anhui Bureau of Geology and Mineral Exploration, Chizhou 247100, China

4. CAS Key Laboratory of Mineralogy and Metallogeny, Guangzhou Institute of Geochemistry, Chinese Academy of Sciences, Guangzhou 510640, China

5. CAS Center for Excellence in Tibetan Plateau Earth Sciences, Beijing 100101

2014-08-22 收稿, 2014-12-28 改回.

Duan LA, Gu HL, Yang XY, Yan ZZ and Sun WD. 2015. Chronology and Hf isotopic study of igneous rocks in the Liwan Cu-polymetal deposit in Guichi along the Middle-Lower Yangtze River. Acta Petrologica Sinica, 31(7) :1943 – 1961

Abstract The Liwan Cu-polymetal deposit is located in Anqing-Guichi ore-cluster area, the Middle-Lower Yangtze River metallogenetic belt. The regional intrusion is mainly composed of potassium-feldspar granite and diorite. The diorite stock is close to the poly-metal mineralization which is concealed underground. The main metallogenetic type is contact metasomatic skarn type. Overall, the Liwan intrusion has high total K₂O + Na₂O contents, low MgO, TiO₂ and P₂O₅ contents, enrichments of large ion lithophile elements (Rb, Th, U), high field strength elements (Zr and Hf, Nb and Y) and light rare earths, depletion in Ba, P, Ti and heavy rare earths. Zircon U-Pb chronology of diorite samples show that intrusion formed in 123.4 ± 2.4 Ma, potassium feldspar granite formed in 122.6 ± 1.3 Ma, reflecting the multiphase characteristics of igneous activity in the Liwan area, these ages are similar to those igneous rocks along the middle-lower Yangtze river around 125 Ma events with A-type granite magmatism and mineralization. All rare earth element distribution patterns of zircon show a typical light rare earth depletion, heavy rare earth enrichment, characteristics of Ce positive anomaly and Eu negative anomaly. Lattice stress model calculation shows relative basaltic diorite andesitic porphyrite and potassium long granite zircon Ce⁴⁺/Ce³⁺ is higher, the mean value of 345, reflecting that it had formed in a relatively high oxygen fugacity environment. Thermometer by zircon Ti calculation shows that the formation of temperature is in the range of 703 ~ 748 °C. Meanwhile, potassium-felspar granite has uniform Hf isotopic compositions of zircon with average of $\varepsilon_{\text{Hf}}(t) = -4.7$, t_{DM2} ranging from 1118 ~ 1356 Ma. The fact that Liwan potassium-feldspar granite has relatively high $\varepsilon_{\text{Hf}}(t)$ values and younger model ages, suggesting the importance of mantle material in the magma source. The inherited zircons in the samples from Liwan basaltic andesitic porphyrite suggest that Palaeoproterozoic basement (2156 Ma) was involved with the generation of Liwan magma. Conjectured from regional geological background, we believe that both the Liwan stock and skarn ore deposit may be formed in tensional function due to plate retreat during subduction of the Pacific plate at about 125 Ma, which is partial melting of residual material products of miscibility with continental-oceanic crust and mantle.

* 本文受国家自然科学基金项目(41173057、41090372、41372087)和安徽省国土资源科技项目(2014-K-04)联合资助。

第一作者简介: 段留安,男,1976 年生,博士生,工程师,矿产勘查及矿床地球化学专业

** 通讯作者:杨晓勇,男,教授,矿床地球化学专业,E-mail: xyyang555@163.com

Key words Copper polymetallic deposit; Liwan; Zircon U-Pb dating; Hf isotope; The Middle-Lower Yangtze River metallogenic belt; Pacific plate subduction

摘要 李湾铜多金属矿位于长江中下游成矿带安庆-贵池矿集区,与矿区岩浆岩有密切的成因联系,是一个典型的矽卡岩型矿床。该区侵入岩主要由钾长花岗岩、闪长岩等组成,总体上具有较高的总碱($K_2O + Na_2O$)和 K_2O 含量,低 MgO 、 TiO_2 和 P_2O_5 含量,富集大离子亲石元素(Rb、Th、U)和高场强元素(Zr、Hf、Nb和Y),亏损Ba、P、Ti,轻稀土富集、亏损重稀土等地球化学特征。通过对闪长岩和钾长花岗岩锆石U-Pb年代学研究表明,前者形成于 123.4 ± 2.4 Ma,后者形成于 122.6 ± 1.3 Ma,这与长江中下游 125 ± 5 Ma岩浆活动及成矿事件一致。两者的锆石稀土元素配分均显示典型的轻稀土亏损、重稀土富集,Ce正异常、Eu负异常特征。前者相对后者锆石的 Ce^{4+}/Ce^{3+} 要高,其均值为345,显示其具有相对较高的氧逸度;锆石Ti温度计计算显示两者形成温度大体一致,为 $703 \sim 748$ °C范围内。同时钾长花岗岩锆石均具有均一的Hf同位素组成, $\epsilon_{Hf}(t)$ 均值为-4.7,二阶段模式年龄为 $1118 \sim 1356$ Ma,较高的 $\epsilon_{Hf}(t)$ 值,指示源区可能有地幔物质的贡献。结合区域地质背景,我们认为该区闪长岩可能是板块后撤过程中残留的洋壳与地幔物质的混合,而附近的钾长花岗岩则是陆壳部分熔融与地幔混溶的结果,两者均位于太平洋板块 125 Ma前后俯冲后撤形成的拉张背景下。

关键词 铜多金属矿;李湾;锆石U-Pb定年;Hf同位素;长江中下游成矿带;太平洋板块俯冲

中图法分类号 P588.121 : P597.3

1 引言

长江中下游成矿带是我国重要的铜金多金属成矿带，一直是地质学家关注的热点地区之一（常印佛等，1991；翟裕生等，1992；Pan and Dong, 1999; Mao *et al.*, 2006; 毛景文等，2009），该成矿带自西向东依次可分为鄂东、九瑞、安庆-贵池、庐枞、铜陵、宁芜和宁镇等7个矿集区（Yang and Lee,

2011; Deng *et al.*, 2011), 李湾铜多金属矿床位于安庆-贵池矿集区之贵池地区(图1a)。已有的研究显示长江中下游铜金成矿作用主要集中在 140 ± 5 Ma, 与燕山期岩浆活动密切相关(Sun *et al.*, 2003; Mao *et al.*, 2006; Wang *et al.*, 2006, 2007; Xie *et al.*, 2009, 2012; Li *et al.*, 2009, 2010; 宋国学等, 2010; 谢建成等, 2012; 周涛发等, 2008, 2012; 段留安等, 2012, 2014)。

近年来安庆-贵池矿集区找矿工作取得了较大进展,如池州市抛刀岭金矿已经是大型规模,并有望达到特大型规模。

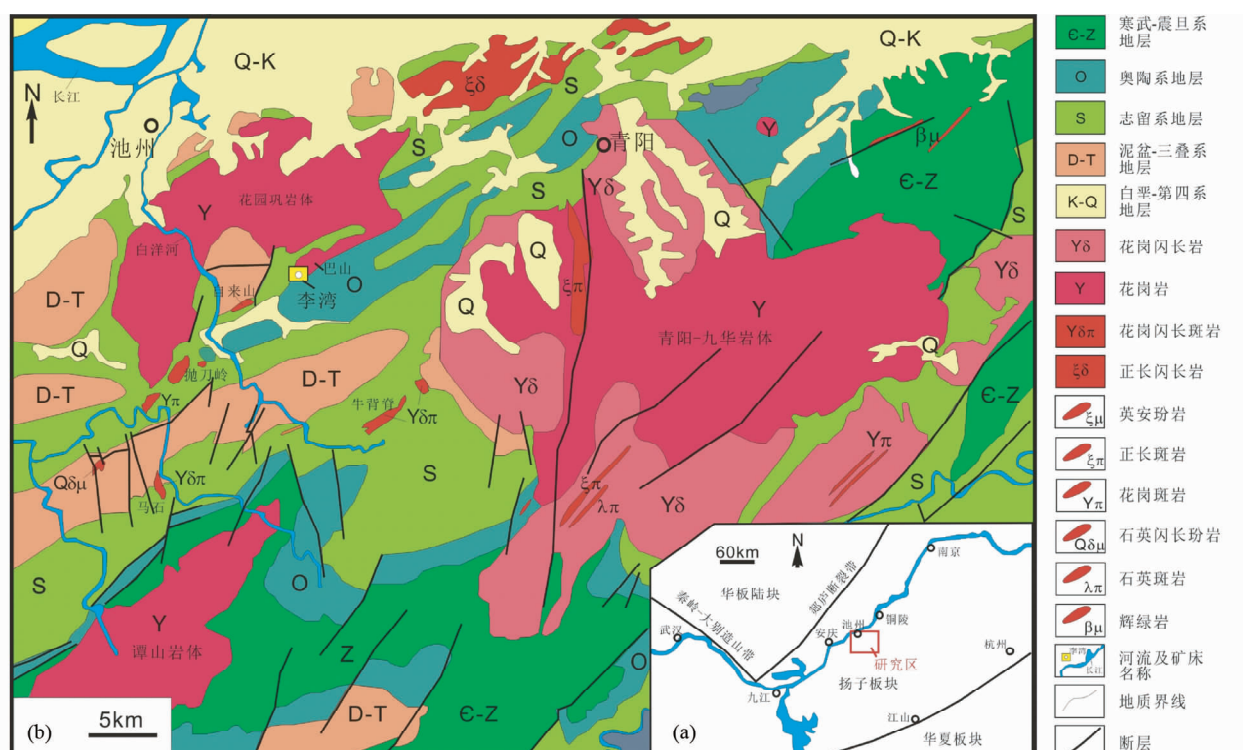


图1 沔州地区区域地质图(据宋国学等, 2010修改)

Fig. 1 Simplified geological map of the Chizhou area (modified after Song *et al.*, 2010).

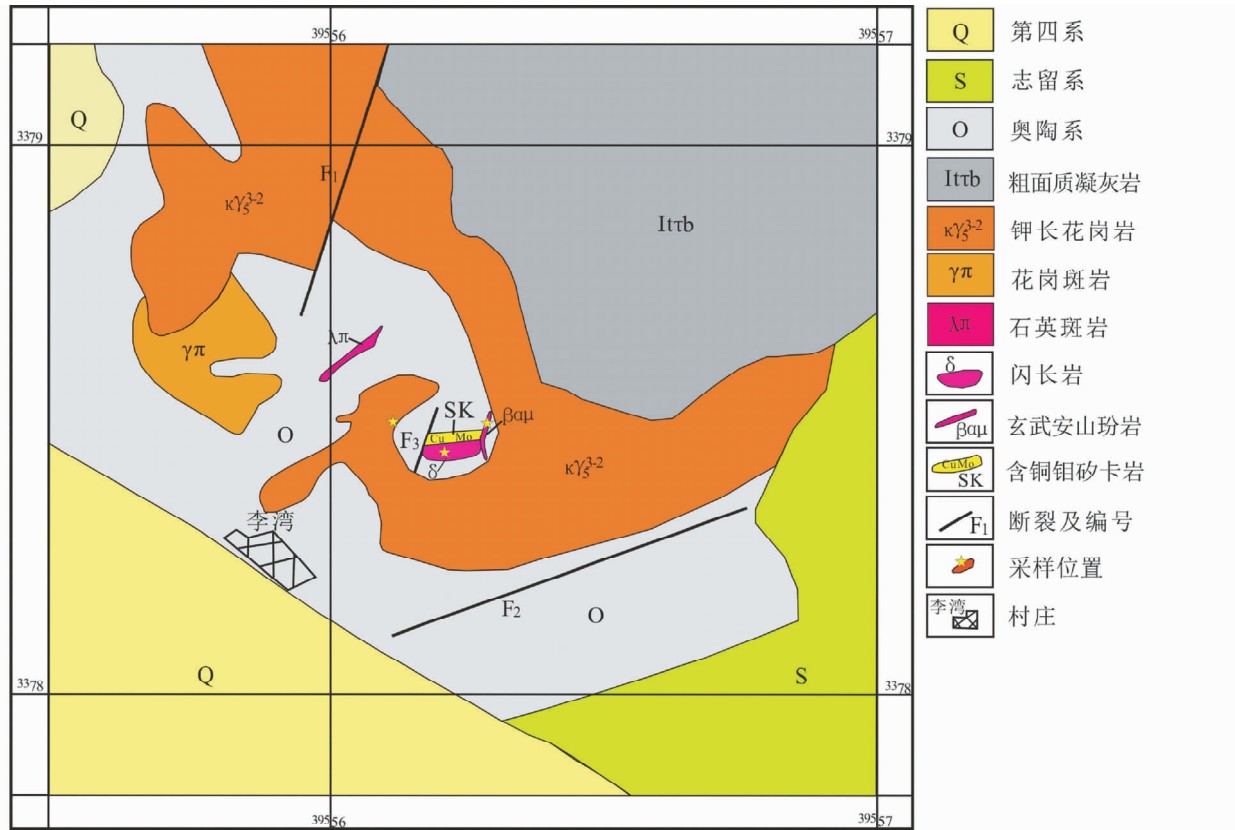


图 2 李湾矿区地质简图

Fig. 2 Geological Map of the Liwan area

(段留安等, 2014)。此外, 池州市黄山岭铅锌矿深部及周边地区、马头铜钼矿、高家榜铜钼矿, 东至赵家岭金矿等找矿工作也取得了较大进展(图 1b)。然而安庆-贵池矿集区基础地质研究相对薄弱。目前人们将研究重点集中在 140 ± 5 Ma 左右的岩浆活动及成矿作用上(宋国学等, 2010; 张智宇等, 2011; 刘圆圆等, 2012; 段留安等, 2012, 2014; 杨贵才等, 2014), 而忽视了 125 ± 5 Ma 左右的岩浆活动及成矿作用。究其原因, 主要源于普遍认为贵池地区花园巩 A 型花岗岩不成矿或成矿差, 以及与 125 ± 5 Ma 时间段目前没有发现大型金属矿产相关。目前为止, 对池州地区 125 ± 5 Ma 左右成矿的矿床实例还没有报道, 由于李湾矿床为接触交代矽卡岩型矿床, 其成矿应接近或晚于成岩年龄, 本文通过对该区与成矿相关的岩浆岩主微量元素、年代学、同位素等研究, 对该地区成岩成矿进行再认识和总结, 进而弥补贵池地区 125 ± 5 Ma 时间段成矿的空缺, 对该区域地质探矿工作提供理论支持。

2 地质背景和矿床地质特征

2.1 区域地质背景

安庆-贵池矿集区位于扬子板块的北东缘、大别造山带与江南地块之间的下扬子台褶带中, 属于贵池-繁昌断褶束

中段, 是大别造山带和江南叠覆造山带相互作用的地区, 其地质构造位置较特殊(图 1a)。该区构造演化大体经历了前寒武纪基底形成、震旦纪-早二叠覆盖沉积和中三叠以来的碰撞造山三个阶段, 随后进入太平洋构造域, 发生了地壳伸展和大规模岩浆活动。

区域地层发育以碳酸盐建造为主、碎屑岩建造为辅的一套沉积盖层, 隶属下扬子地层分区贵池地层小区。古生代-早三叠世地层是本区 W、Mo、Pb、Zn、Cu、Au、Ag 等金属矿床主要的容矿层位(唐永成等, 1998), 本区地层对矿床的控制作用主要表现在矿化类型上的差异, 如志留系砂页岩地层易形成斑岩型、热液型矿化及蚀变岩型矿化(段留安等, 2013), 奥陶系、石炭系碳酸盐岩地层易形成矽卡岩型和热液型矿化(董胜, 2006)。该区燕山期岩浆岩发育, 以中深-浅成侵入岩为主, 大规模的岩体有青阳-九华岩体(750 km^2 , $139 \sim 142$ Ma)、谭山岩体(140 km^2 , $129 \sim 133$ Ma)、花园巩岩体(220 km^2 , 125 Ma)(Wu et al., 2012), 均呈大型岩基产出的复式岩体, 分布于区内的中东部(图 1b), 岩石类型主要为花岗闪长岩、二长花岗岩和钾长花岗岩。小规模的有马石、抛刀岭、乌石、牛脊背等岩体, 多呈小岩株产出, 出露面积一般不足 2 km^2 (图 1b), 多属深熔高钾钙碱性系列, 与铜多金属矿密切相关。花园巩岩体为 A 型花岗岩类岩体, 一般认为是沿江地区中生代岩浆活动的最后阶段产物, 岩石偏碱性, 成矿



图3 李湾矿区各类岩矿石照片

(a) 钾长花岗岩; (b) 闪长岩; (c) 安山玄武玢岩; (d) 含多金属矽卡化闪长岩; (e) 含辉钼矿闪长岩; (f) 含黄铁矿条带状矿石; (g, h) 多金属矽卡岩; (i) 钾长花岗岩中的闪长岩捕掳体

Fig. 3 Field photographs for Liwan area

(a) moyite; (b) diorite; (c) basaltic-andesitic porphyry; (d) multi-metal contained skarn diorite; (e) molybdenite bearing diorite; (f) pyrite bearing band ore; (g, h) polymetallic ore bearing skarn; (i) diorite xenoliths in the moyite

作用较差(董胜, 2006)。

区域地质构造处于贵池背斜带之自来山背斜西段核部, 巴山岩体西南外围。自来山背斜总体呈北东-南西延伸, 核部地层为奥陶系仑山组下段白云岩, 北西翼因岩体侵入破坏支离破碎, 南东翼出露地层为奥陶系下统仑山组上段灰岩至志留系高家边组砂页岩, 地层倾向南东, 倾角 $44^{\circ} \sim 65^{\circ}$ 。沿自来山背斜核部常出露有中酸性花岗斑岩、花岗闪长斑岩等侵入岩, 在岩体与围岩的接触带蚀变-交代作用强烈, 局部产出铜多金属矿体。

2.2 矿区地质

李湾矿区出露地层为奥陶纪和志留纪地层(图2)。矿区内除褶皱构造外, 断裂构造也十分发育, 主要有 F_1 、 F_2 和 F_3 三条断裂。 F_1 断裂位于矿区西北侧边缘, 为左旋平移断层, 呈北北东向展布, 为区域性梅村-墩上大断层的一部分; F_2 断裂位于本区南侧边缘, 为北东向展布的逆断层, 断层北

盘为仑山组上、下段灰岩、白云岩, 南盘为红花园、大湾组等地层, 断层走向长约4.5km, 两端均出勘查区外, 断层倾向南东, 倾角约 50° ; F_3 断裂仅在探矿坑道中见到, 推测规模较小, 倾向南东 120° , 倾角约 70° , 为成岩前正断层, 成矿岩体西延受阻, 矿化就此中断, 断层带较窄, 发育有角砾岩。

矿区岩浆岩发育, 岩浆岩侵位受自来山背斜构造和北北东左旋平行断层的控制, 形成浅成侵入岩体和次火山岩体。其中次火山岩, 发育于矿区的北部, 岩性为粗面质熔结角砾凝灰岩, 覆盖于花岗斑岩和白云岩之上; 侵入岩岩性主要为钾长花岗岩(图3a, i)、石英斑岩、花岗斑岩、闪长岩(图3b)及玄武安山玢岩脉(图3c)等。钾长花岗岩在矿区出露较广, 局部见有闪长岩捕虏体(图3i), 其与地层接触带未见明显金属矿化; 安山玄武玢岩仅在+72m水平坑道中发现, 呈近南北向向西突出的弧状展布, 倾向西或西北, 倾角 70° , 宽 $2 \sim 3$ m, 构成了主矿体东部边界; 闪长岩地表未见出露, 仅在坑道和钻孔中见到, 从野外地质特征看, 与本区铜多金属矿

密切相关。闪长岩与围岩的接触带表现出强烈的蚀变和铜-钼-锌等多金属矿化(图 3d-f), 同时闪长岩内部有时也见有黄铜矿、斑铜矿、闪锌矿、黄铁矿、辉钼矿等金属矿化(图 3d, e)。

李湾矿区多年来民企一直在采矿中, 从钻孔、坑道及采掘出来的岩矿石看该矿床属于小而富的矽卡岩型铜多金属矿, 其矿石类型为含铜黄铁矿、含铜硫矽卡岩、含铅锌矽卡岩等, 矿石的主要有益组分为 Cu、S, 个别矿体含 Mo、Pb、Zn、Fe。目前, 经稀疏钻探及坑探控制矿体 10 个, 但多没有完全控制。如Ⅱ号矿体, 由 ZK803 等 3 个钻孔控制, 走向 NEE, 地表延伸 56m, 倾向 SE, 倾角 60°, 斜深 200m, 斜深大于延伸(斜深尚未完全控制)。矿体最大厚度 16.94m, 最小厚度 1.08m, 平均厚度 6.96m, 铜平均品位 0.62%, 硫平均品位 17.34%, 铜硫矿体赋存标高为 -106 ~ 76m; Ⅵ号矿体, 由 ZK801、ZK803 控制, 总体呈透镜状, 向上有分枝, 倾向 SE, 倾角 45°, 斜深 106m, 最大厚度 22.02m, 最小厚度 4.16m, 平均厚度 14.35m, 厚度变化系数为 64.06%, 属较稳定矿体。铜平均品位 0.70%, 硫平均品位 13.90%, 铜硫矿体赋存标高 -114 ~ -176m。

从区域成矿条件分析, 李湾一带铜多金属具有较好的成矿前景, 已知的地质特征及坑道采出的闪长岩中发育的铜、钼矿化等信息也显示, 浅部的闪长岩与地层的接触带形成高硫矽卡岩型铜多金属矿, 而在深部可能具有斑岩型铜钼矿的找矿潜力。

3 样品采集、加工及测试结果

为了揭示李湾矿区岩浆岩的地球化学特征及与铜多金

属成矿作用的关系, 本文对矿区的钾长花岗岩、闪长岩及玄武安山玢岩进行了主量元素、微量元素、单颗粒锆石 U-Pb 定年和锆石原位 Hf 同位素分析。

全岩的主量元素和微量元素分析在广州澳实矿物实验室完成。其中常量元素采用 ME-XRF06 法, 由 X 荧光光谱仪测定, 分析流程见刘颖等(1996); 稀土元素采用 ME-MS81 法, 由等离子体质谱测定; 微量元素采用 ME-MS61 法, 由等离子体质谱测定, 具体分析流程见 Qi *et al.* (2000)。

锆石单矿物分选由河北省地勘局廊坊实验室完成, 将 8 ~ 10kg 重的原岩样品粉碎, 经常规重选和电磁选后在双目镜下挑选锆石。双目镜下将分选好的锆石根据颜色、自形程度、形态等特征初步分类, 挑选出具有代表性的锆石用环氧树脂制靶、打磨和抛光。样品测定之前用体积百分比为 3% 的 HNO₃ 清洗样品表面, 以除去样品表面的污染。然后进行锆石显微镜照相(反射光和透射光)和阴极发光(CL)照相, 锆石的透反射和阴极发光照相在中国科学技术大学壳-幔物质与环境重点实验室完成。

锆石的激光剥蚀电感耦合等离子体质谱(LA-ICP-MS)原位 U-Pb 定年和微量元素分析在中国科学院广州地球化学研究所同位素地球化学国家重点实验室完成。仪器组成及实验参数见 Li *et al.* (2012)。数据处理采用 ICPMSDataCal 软件(Liu *et al.*, 2008, 2010a), 年龄计算采用 ISOPLOT(3.00 版)软件(Ludwig, 2003)进行。详细分析方法见 Yuan *et al.* (2004) 和 Liu *et al.* (2010a)。

锆石的微区原位 Lu-Hf 同位素分析在西北大学大陆动力学国家重点实验室完成。所用质谱为 Nu Plasma 型多接收电感耦合等离子体质谱(MC-ICP-MS), 激光剥蚀系统为 193nm ArF 准分子激光器的 GeoLas 2005。激光束直径为 44 μm, 激光脉冲频率为 8Hz。具体分析方法和仪器参数详见

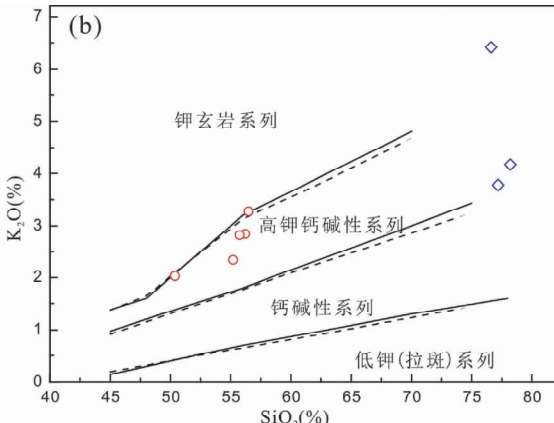
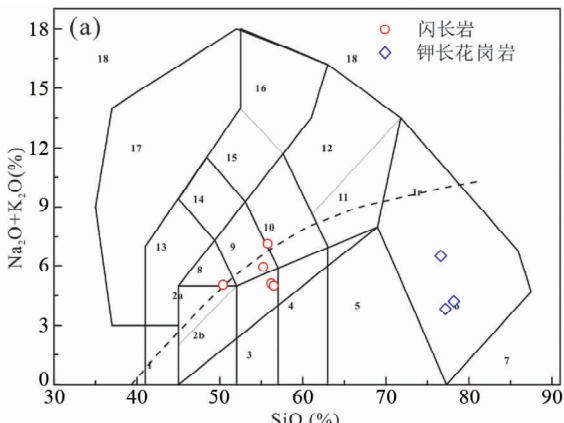


图 4 李湾矿区侵入岩地球化学判别图解

(a) SiO₂-Na₂O + K₂O 判别图解(据 Le Base *et al.*, 1986); (b) 岩石系列 SiO₂-K₂O 图解(实线据 Peccerillo and Taylor, 1976; 虚线据 Middlemost, 1985)

Fig. 4 Geochemical discrimination plot of the Liwan intrusions

(a) SiO₂ vs. Na₂O + K₂O plot (after Le Base *et al.*, 1986); (b) K₂O vs. SiO₂ diagram (solid lines after Peccerillo and Taylor, 1976; dashed line after Middlemost, 1985)

表 1 李湾矿区侵入岩全岩主量组成(wt%)

Table 1 Rock major element data for the Liwan intrusions (wt%)

| 样品号 | LW1-1 | LW1-2 | LW1-3 | LW1-4 | LW1-5 | LW2-1 | LW2-2 | LW2-3 | LW2-4 | LW2-5 | LW3-1 | LW3-2 | LW3-3 |
|---|--------|-------|-------|-------|-------|-------|-------|-------|--------|--------|-------|-------|--------|
| 岩性 | 玄武安山玢岩 | | | | | 闪长岩 | | | | | 钾长花岗岩 | | |
| SiO ₂ | 43.88 | 42.54 | 43.11 | 43.21 | 42.00 | 51.70 | 50.76 | 52.50 | 45.73 | 52.35 | 74.38 | 74.61 | 73.29 |
| TiO ₂ | 0.79 | 0.86 | 0.81 | 0.87 | 0.87 | 1.36 | 1.31 | 1.43 | 1.68 | 1.38 | 0.21 | 0.18 | 0.18 |
| Al ₂ O ₃ | 22.83 | 22.51 | 23.14 | 24.7 | 25.14 | 17.12 | 16.69 | 17.55 | 16.07 | 17.05 | 13.07 | 12.82 | 12.61 |
| Fe ₂ O ₃ ^T | 3.40 | 2.65 | 2.19 | 1.78 | 2.19 | 6.83 | 6.97 | 7.99 | 10.57 | 7.26 | 1.38 | 1.24 | 1.35 |
| MnO | 0.10 | 0.12 | 0.11 | 0.09 | 0.10 | 0.09 | 0.11 | 0.09 | 0.14 | 0.11 | 0.05 | 0.05 | 0.08 |
| MgO | 3.90 | 4.09 | 4.25 | 4.14 | 2.94 | 4.19 | 3.11 | 3.82 | 3.04 | 2.46 | 0.49 | 0.57 | 0.54 |
| CaO | 18.67 | 20.27 | 18.19 | 18.71 | 22.35 | 5.15 | 6.67 | 4.01 | 8.27 | 5.65 | 1.12 | 1.88 | 3.24 |
| Na ₂ O | 0.79 | 0.54 | 0.55 | 0.68 | 0.53 | 2.08 | 3.31 | 1.61 | 2.74 | 4.05 | 0.09 | 0.03 | 0.03 |
| K ₂ O | 0.45 | 1.12 | 1.89 | 1.01 | 0.21 | 2.62 | 2.15 | 3.04 | 1.84 | 2.65 | 6.23 | 3.98 | 3.59 |
| P ₂ O ₅ | 0.29 | 0.29 | 0.28 | 0.29 | 0.31 | 0.82 | 0.80 | 0.86 | 0.56 | 0.83 | 0.03 | 0.09 | 0.03 |
| LOI | 3.29 | 3.77 | 4.46 | 3.24 | 3.09 | 7.98 | 7.68 | 6.63 | 9.26 | 6.26 | 2.77 | 4.28 | 5.28 |
| Total | 98.45 | 98.87 | 99.10 | 98.86 | 99.80 | 99.97 | 99.61 | 99.57 | 100.04 | 100.15 | 99.85 | 99.68 | 100.23 |

表 2 李湾矿区侵入岩微量元素组成(× 10⁻⁶)Table 2 Trace elements data for the Liwan intrusions (× 10⁻⁶)

| 样品号 | LW1-1 | LW1-2 | LW1-3 | LW1-4 | LW1-5 | LW2-1 | LW2-2 | LW2-3 | LW2-4 | LW2-5 | LW3-1 | LW3-2 | |
|-----|--------|-------|-------|-------|-------|-------|-------|-------|-------|-------|-------|-------|--|
| 岩性 | 玄武安山玢岩 | | | | | 闪长岩 | | | | | 钾长花岗岩 | | |
| Ba | 52.0 | 96.70 | 81.80 | 102.5 | 39.60 | 75.30 | 115.0 | 142.5 | 630.0 | 570.0 | 193.5 | 83.9 | |
| Ce | 276.0 | 124.0 | 142.5 | 185.5 | 208.0 | 107.5 | 123.5 | 121.5 | 79.9 | 130.0 | 136.0 | 125.5 | |
| Co | 3.8 | 1.3 | 1.0 | 2.0 | 1.8 | 12.6 | 11.8 | 13.3 | 31.8 | 12.5 | 0.6 | 0.5 | |
| Cr | 30 | 50 | 20 | 60 | 20 | <10 | <10 | <10 | <10 | <10 | <10 | <10 | |
| Cs | 4.1 | 5.0 | 21.9 | 9.8 | 1.6 | 24.7 | 10.1 | 12.5 | 4.2 | 8.9 | 8.9 | 10.4 | |
| Cu | 3990 | 79 | 81 | 1560 | 375 | 13 | 12 | <5 | 24 | <5 | <5 | 6 | |
| Dy | 5.0 | 4.1 | 3.9 | 4.4 | 4.2 | 7.4 | 6.8 | 7.0 | 5.9 | 7.0 | 8.0 | 7.5 | |
| Er | 2.3 | 2.2 | 1.9 | 1.9 | 2.0 | 4.0 | 3.6 | 3.9 | 3.3 | 3.8 | 6.1 | 6.0 | |
| Eu | 5.0 | 1.9 | 2.0 | 2.4 | 3.1 | 2.6 | 2.6 | 2.7 | 2.3 | 2.8 | 0.6 | 0.5 | |
| Ga | 62.7 | 46.8 | 53.1 | 53.2 | 53.9 | 23.3 | 20.6 | 22.9 | 20.6 | 21.7 | 26.1 | 26.9 | |
| Gd | 12.4 | 6.7 | 6.6 | 8.7 | 8.6 | 9.2 | 8.9 | 9.3 | 7.1 | 9.5 | 6.9 | 6.4 | |
| Hf | 6.9 | 7.3 | 7.8 | 8.0 | 8.4 | 7.0 | 6.6 | 7.3 | 5.0 | 7.0 | 11.9 | 12.2 | |
| Ho | 0.8 | 0.8 | 0.7 | 0.7 | 0.7 | 1.4 | 1.3 | 1.4 | 1.1 | 1.3 | 1.8 | 1.7 | |
| La | 166.5 | 75.6 | 86.8 | 108.0 | 116.5 | 51.2 | 60.5 | 57.4 | 38.4 | 63.9 | 73.2 | 68.3 | |
| Lu | 0.2 | 0.2 | 0.2 | 0.2 | 0.2 | 0.5 | 0.5 | 0.5 | 0.5 | 0.5 | 1.3 | 1.3 | |
| Mo | 3600 | 30 | 1785 | 8 | 2030 | 7 | 4 | 2 | 2 | <2 | 9 | 2 | |
| Nb | 19.8 | 28.4 | 31.1 | 29.1 | 29.9 | 22.9 | 21.8 | 23.5 | 12.6 | 22.3 | 68.4 | 68.7 | |
| Nd | 103.5 | 46.1 | 51.7 | 69.0 | 80.1 | 50.6 | 54.6 | 53.8 | 38.6 | 58.3 | 39.1 | 34.7 | |
| Ni | 11 | 49 | <5 | 26 | <5 | <5 | <5 | <5 | 10 | <5 | <5 | <5 | |
| Pb | 18 | 16 | 19 | 18 | 21 | 12 | 5 | 5 | 8 | 8 | 10 | 6 | |
| Pr | 30.2 | 13.4 | 15.4 | 20.2 | 23.2 | 12.9 | 14.6 | 14.3 | 9.7 | 15.2 | 13.0 | 11.9 | |
| Rb | 29.0 | 60.8 | 100.5 | 60.7 | 12.2 | 169.0 | 93.5 | 155.0 | 62.0 | 111.5 | 345.0 | 254.0 | |
| Sm | 16.3 | 7.2 | 7.8 | 10.7 | 11.2 | 10.1 | 10.1 | 10.4 | 7.5 | 10.6 | 6.9 | 6.0 | |
| Sn | 41 | 46 | 42 | 26 | 36 | 2 | 2 | 2 | 1 | 2 | 5 | 5 | |
| Sr | 587 | 808 | 973 | 1155 | 545 | 225 | 340 | 192 | 605 | 298 | 61.7 | 50 | |
| Ta | 1.6 | 1.9 | 2.2 | 2.1 | 2.1 | 1.2 | 1.2 | 1.3 | 0.7 | 1.2 | 4.9 | 4.9 | |
| Tb | 1.3 | 0.9 | 0.8 | 1.0 | 0.9 | 1.3 | 1.2 | 1.3 | 1.1 | 1.3 | 1.2 | 1.1 | |
| Th | 10.6 | 10.4 | 10.8 | 9.2 | 12.8 | 8.6 | 8.2 | 8.9 | 5.4 | 8.5 | 59.8 | 60.2 | |
| Tl | 0.5 | <0.5 | <0.5 | <0.5 | <0.5 | 0.6 | <0.5 | 0.6 | <0.5 | <0.5 | 1.5 | 0.7 | |
| Tm | 0.3 | 0.3 | 0.3 | 0.3 | 0.3 | 0.5 | 0.5 | 0.6 | 0.5 | 0.5 | 1.1 | 1.0 | |
| U | 5.8 | 3.6 | 3.7 | 3.9 | 5.2 | 2.2 | 2.3 | 2.2 | 1.2 | 2.2 | 17.3 | 16.3 | |
| V | 98 | 76 | 76 | 68 | 66 | 109 | 102 | 111 | 219 | 104 | 7 | 6 | |
| W | 8820 | 184 | 35 | 265 | 870 | 12 | 14 | 8 | 2 | 14 | 11 | 10 | |
| Y | 22.4 | 20.4 | 18.3 | 18.8 | 19.5 | 37.7 | 33.3 | 35.4 | 29.9 | 34.9 | 53.8 | 52.6 | |
| Yb | 1.6 | 1.8 | 1.6 | 1.4 | 1.6 | 3.4 | 3.3 | 3.4 | 3.0 | 3.4 | 7.7 | 7.4 | |
| Zn | 110 | 48 | 49 | 105 | 79 | 130 | 100 | 122 | 135 | 109 | 33 | 35 | |
| Zr | 264 | 273 | 291 | 296 | 316 | 304 | 287 | 309 | 207 | 300 | 311 | 324 | |

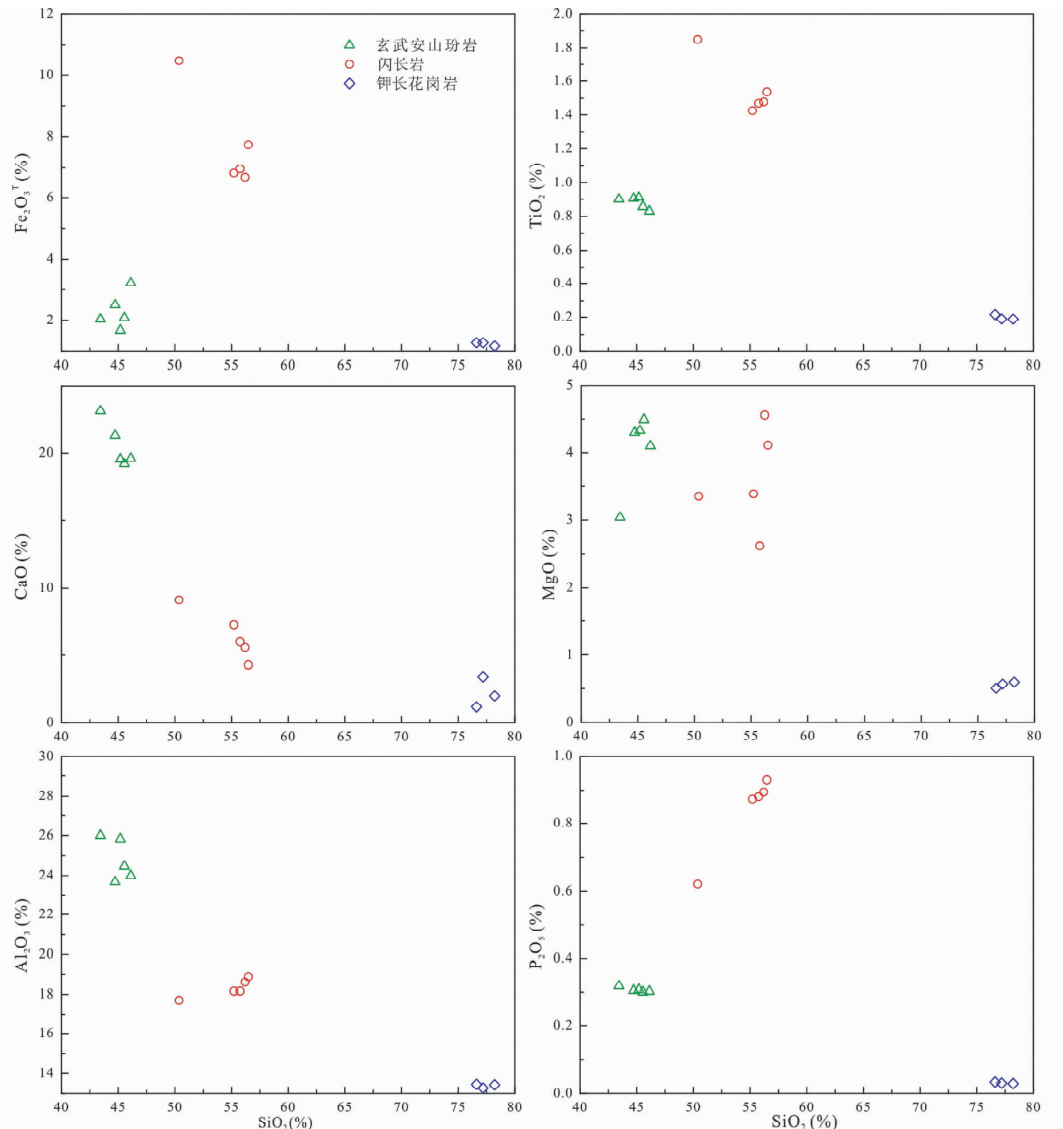


图 5 李湾矿区侵入岩 Harker 图解

Fig. 5 Harker major element variation diagrams of Liwan intrusions

Yuan *et al.* (2008)。用¹⁷⁶Lu/¹⁷⁵Lu = 0.02655 (De Biévre and Taylor, 1993) 和¹⁷⁶Yb/¹⁷²Yb = 0.58545 (Chu *et al.*, 2001) 作为校正因子来进行同质异位干扰校正, 计算样品的¹⁷⁶Lu/¹⁷⁷Hf 和¹⁷⁶Hf/¹⁷⁷Hf。以标准锆石 MON-1、GJ-1、91500 作为外标, 其推荐的标准值依次为 0.282739 ± 0.000057, 0.282015 ± 0.000056, 0.282307 ± 0.000055。在进行 $\varepsilon_{\text{Hf}}(t)$ 计算时, 采用¹⁷⁶Lu 衰变常数 = $1.867 \times 10^{-11} \text{ year}^{-1}$ (Soderlund *et al.*, 2004), 球粒陨石现今的¹⁷⁶Hf/¹⁷⁷Hf = 0.282772 和¹⁷⁶Lu/¹⁷⁷Hf = 0.0332 (Blichert and Albarede, 1997)。在进行模式年龄计算时, 采用现今的亏损地幔¹⁷⁶Hf/¹⁷⁷Hf = 0.28325 和¹⁷⁶Lu/¹⁷⁷Hf = 0.0384 (Griffin *et al.*, 2000), 现今平均大陆壳的¹⁷⁶Lu/¹⁷⁷Hf = 0.015 (Griffin *et al.*, 2002)。

4 分析结果

4.1 元素地球化学特征

主要元素分析结果见表 1, 微量元素分析结果见表 2。

闪长岩具较低的 SiO₂ (45.73% ~ 52.5%, 平均为 50.61%) 和 Fe₂O₃^T (6.83% ~ 10.57%, 平均为 7.92%) 含量; 全碱含量 (K₂O + Na₂O) 为 4.58% ~ 6.7%, 平均为 5.22%; Mg[#] 值为 36.3 ~ 54.86, 平均为 45.38, CaO 含量为 4.01% ~ 8.27%, 平均为 5.95%。在 TAS 图中, 落入闪长岩范围 (图 4a), 岩石具有富铝、镁特征, 属于高钾钙碱性系列 (图 4b)。

钾长花岗岩具有较高的 SiO₂ (73.29% ~ 74.61%, 平均

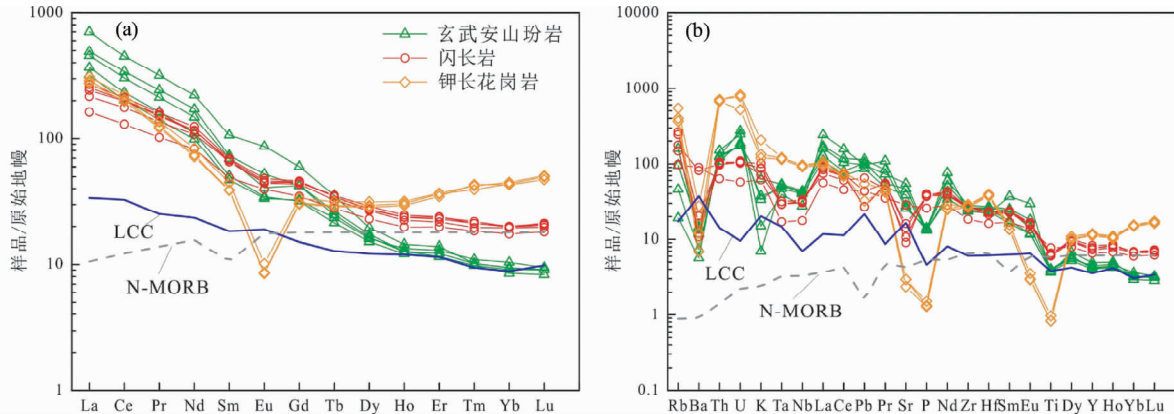


图6 李湾矿区岩浆岩稀土元素配分图(a)及微量元素蛛网图(b)(球粒陨石标准值据 Sun and McDonough, 1989; 原始地幔及其他地质储库标准值据 McDonough and Sun, 1995)

Fig. 6 Chondrite-normalized REE patterns (a) and primitive mantle-normalized trace elements patterns (b) of Liwan intrusions (chondrite values are from Sun and McDonough, 1989; primitive mantle and other geological storage standard values are from McDonough and Sun, 1995)

为 74.09%)、 Al_2O_3 (12.61% ~ 13.07%, 平均为 12.83%) 和 Fe_2O_3^T (1.24% ~ 1.38%, 平均为 1.32%) 含量; 全碱 ($\text{K}_2\text{O} + \text{Na}_2\text{O}$) 含量为 3.62% ~ 6.32%, 平均为 4.65%; TiO_2 含量为 0.18% ~ 0.21%, 平均为 0.19%; MgO 含量为 0.49% ~ 0.57%, 平均为 0.53%; $\text{Mg}^#$ 值为 41.29 ~ 47.66, 平均为 44.39; CaO 含量为 1.12% ~ 3.24%, 平均为 2.08%。在 TAS 图中, 落入花岗岩范围(图 4a), 属于高钾钙碱性系列。

玄武安山玢岩具有较低的 SiO_2 含量 (42% ~ 43.88%, 平均为 42.95%), 较高的 Al_2O_3 含量 (22.51% ~ 25.14%, 平均为 23.66%)。 Fe_2O_3^T 含量为 1.78% ~ 3.4%, 平均为 2.44%; $\text{K}_2\text{O} + \text{Na}_2\text{O}$ 含量为 0.74% ~ 2.44%, 平均为 1.55%; TiO_2 含量为 0.79% ~ 0.87%, 平均为 0.84%; MgO 含量为 2.94% ~ 4.25%, 平均为 3.86%; $\text{Mg}^#$ 值为 69.44 ~ 82.17, 平均为 75.80; CaO 含量为 18.19% ~ 22.35%, 平均为 19.64%。

李湾矿区侵入岩 A/CNK 比值为 1.03 ~ 2.18, 显示强过铝质的特征。Harker 图解中 Al_2O_3 、 Fe_2O_3^T 、 CaO 、 P_2O_5 、 TiO_2 与 SiO_2 存在负相关性(图 5), 表明在岩石形成过程中发生斜长石、辉石、角闪石、钛铁矿的分离结晶作用。

钾长花岗岩 ΣREE 为 269.4×10^{-6} ~ 302.7×10^{-6} , 平均值为 283.8×10^{-6} 。其 LREE/HREE 值为 7.54 ~ 7.91, 平均值为 7.69。(La/Yb)_N 的值为 6.48 ~ 6.86, 平均值为 6.65; 闪长岩 ΣREE 为 198.7×10^{-6} ~ 308.1×10^{-6} , 平均值为 269.7×10^{-6} 。其 LREE/HREE 值为 7.06 ~ 10.26, 平均值为 9.27。(La/Yb)_N 的值为 9.30 ~ 13.40, 平均值为 11.77; 玄武安山玢岩 ΣREE 为 285.1×10^{-6} ~ 621.4×10^{-6} , 平均值为 420.7×10^{-6} , 变化范围较大。其 LREE/HREE 值为 15.95 ~ 25.04, 平均值为 21.07。(La/Yb)_N 的值为 30.64 ~ 74.64, 平均值为 50.30。玄武安山玢岩稀土总量高, 轻重稀土分异明显, 轻稀土显著偏高, 可能是受到了俯冲流体交代作用。三

者整体上具有富集轻稀土、亏损重稀土, 轻重稀土分异明显的特点。钾长花岗岩表现出明显的 Eu 负异常(图 6a), 表明源区具有斜长石的分离结晶。稀土配分模式右倾型不同于一般的从地幔分离出来的岩石稀土配分模式(如 MORB)(图 6a), 说明李湾钾长花岗岩岩浆源区并不是从原始地幔或者亏损软流圈地幔分离出来的, 而可能是从岩石圈地幔分离的产物。

钾长花岗岩具有典型的 A 型花岗岩特征: 高总碱 ($\text{K}_2\text{O} + \text{Na}_2\text{O}$) 和 K_2O 含量 (3.59% ~ 6.23%), 低 MgO 、 TiO_2 和 P_2O_5 含量, 富集大离子亲石元素 (Rb、Th、U) 和高场强元素 (Zr、Hf、Nb 和 Y), 亏损 Ba、P、Ti(图 6b)。在 A 型花岗岩判别图解中(图 7), 李湾钾长花岗岩落入 A 型花岗岩区域, 这与区域花园巩 A 型花岗岩一致。

4.2 同位素年代学

锆石定年分析结果见表 3。

李湾矿区钾长花岗岩锆石多为无色透明-浅黄色自形晶体, 多呈长柱状, 长宽比多介于 1:1 ~ 3:1。CL 照片显示多数锆石震荡环带发育, Th/U 比值均大于 0.4。这些特征表明其为岩浆成因锆石(Hoskin, 2000; Sun et al., 2002; 吴元保和郑永飞, 2004)。27 颗锆石的 $^{206}\text{Pb}/^{238}\text{U}$ 表面年龄为 $117 \pm 2\text{Ma}$ ~ $130 \pm 2\text{Ma}$, 加权平均年龄为 $122.6 \pm 1.3\text{Ma}$ (图 8a); 玄武安山玢岩大部分都是继承锆石, $^{206}\text{Pb}/^{238}\text{U}$ 表面年龄为 $151.6 \pm 5\text{Ma}$ ~ $2156.4 \pm 43\text{Ma}$ (图 8b); 闪长岩锆石多为无色透明-浅黄色自形晶体, 多为长柱状, 长宽比多介于 1:1 ~ 3:1。CL 照片显示多数锆石震荡环带发育, 为典型岩浆成岩锆石(Hoskin, 2000; Sun et al., 2002; 吴元保和郑永飞, 2004), 其 $^{206}\text{Pb}/^{238}\text{U}$ 年龄变化于 $116.8 \pm 2\text{Ma}$ ~ $147.1 \pm 2\text{Ma}$ 之间, 加权平均年龄为 $123.4 \pm 2.4\text{Ma}$ (图 8c), 说明闪长岩侵位比钾长花岗岩稍早一点, 这从野外见钾长花岗岩中含有闪长岩的

表 3 李湾矿区岩浆岩锆石 LA-ICP-MS U-Pb 定年分析结果

Table 3 LA-ICP-MS zircon U-Pb data of the Liwan intrusions

| 测点号 | Th | U | Th/U | $^{207}\text{Pb}/^{235}\text{U}$ | 1σ | $^{206}\text{Pb}/^{238}\text{U}$ | 1σ | $^{206}\text{Pb}/^{238}\text{U}$ | 1σ |
|---------------|----------------------|----------------------|------|----------------------------------|-----------|----------------------------------|-----------|----------------------------------|-----------|
| | ($\times 10^{-6}$) | ($\times 10^{-6}$) | | ($\times 10^{-6}$) | | (Ma) | | ($\times 10^{-6}$) | |
| 闪长岩 | | | | | | | | | |
| LW2-1-1 | 926 | 919 | 1.01 | 0.1078 | 0.0080 | 0.0183 | 0.0003 | 117 | 2 |
| LW2-1-2 | 299 | 555 | 0.54 | 0.1316 | 0.0135 | 0.0199 | 0.0004 | 127 | 3 |
| LW2-1-3 | 453 | 1054 | 0.43 | 0.1403 | 0.0101 | 0.0216 | 0.0006 | 138 | 4 |
| LW2-1-4 | 114 | 167 | 0.68 | 0.1432 | 0.0166 | 0.0184 | 0.0006 | 118 | 4 |
| LW2-1-5 | 145 | 292 | 0.50 | 0.1244 | 0.0142 | 0.0208 | 0.0006 | 132 | 4 |
| LW2-1-10 | 1149 | 1061 | 1.08 | 0.0832 | 0.0078 | 0.0186 | 0.0005 | 119 | 3 |
| 玄武安山玢岩 | | | | | | | | | |
| LW1-1-1 | 500 | 538 | 0.93 | 0.9106 | 0.0487 | 0.0984 | 0.0021 | 605 | 12 |
| LW1-1-2 | 59 | 418 | 0.14 | 0.4834 | 0.0309 | 0.0606 | 0.0018 | 379 | 11 |
| LW1-1-5 | 181 | 347 | 0.52 | 0.1509 | 0.0170 | 0.0238 | 0.0008 | 152 | 5 |
| LW1-1-6 | 276 | 210 | 1.31 | 3.5826 | 0.2437 | 0.2417 | 0.0111 | 1395 | 58 |
| LW1-1-7 | 31 | 43 | 0.72 | 1.5948 | 0.1242 | 0.1843 | 0.0045 | 1090 | 25 |
| LW1-1-9 | 118 | 137 | 0.87 | 0.5755 | 0.0595 | 0.0731 | 0.0036 | 455 | 21 |
| LW1-1-10 | 242 | 645 | 0.38 | 5.1376 | 0.3406 | 0.2958 | 0.0049 | 1671 | 24 |
| LW1-1-11 | 557 | 1332 | 0.42 | 1.6546 | 0.0936 | 0.1591 | 0.0037 | 952 | 21 |
| LW1-1-13 | 131 | 173 | 0.76 | 1.0549 | 0.0769 | 0.1129 | 0.0035 | 690 | 20 |
| LW1-1-14 | 211 | 155 | 1.36 | 7.4045 | 0.4916 | 0.3541 | 0.0137 | 1954 | 65 |
| LW1-1-15 | 164 | 122 | 1.34 | 4.8226 | 0.2844 | 0.3101 | 0.0097 | 1741 | 48 |
| LW1-1-16 | 70 | 557 | 0.13 | 0.2929 | 0.0198 | 0.0348 | 0.0008 | 221 | 5 |
| LW1-1-18 | 103 | 331 | 0.31 | 0.3892 | 0.0297 | 0.0502 | 0.0017 | 316 | 10 |
| LW1-1-19 | 588 | 383 | 1.54 | 0.9956 | 0.0567 | 0.1191 | 0.0032 | 725 | 19 |
| LW1-1-20 | 55 | 179 | 0.31 | 8.0630 | 0.3915 | 0.3973 | 0.0093 | 2156 | 43 |
| LW1-1-21 | 23 | 45 | 0.51 | 1.0773 | 0.1020 | 0.1225 | 0.0027 | 745 | 16 |
| LW1-1-22 | 48 | 47 | 1.02 | 0.8367 | 0.1034 | 0.1040 | 0.0038 | 638 | 22 |
| LW1-1-23 | 440 | 343 | 1.28 | 1.0611 | 0.0518 | 0.1289 | 0.0017 | 782 | 10 |
| LW1-1-25 | 319 | 480 | 0.66 | 0.8021 | 0.0481 | 0.0914 | 0.0035 | 564 | 21 |
| LW1-1-26 | 83 | 137 | 0.60 | 1.7326 | 0.1176 | 0.1623 | 0.0059 | 970 | 32 |
| LW1-1-27 | 339 | 486 | 0.70 | 1.2467 | 0.0549 | 0.1154 | 0.0025 | 704 | 15 |
| LW1-1-30 | 104 | 142 | 0.73 | 5.0082 | 0.3001 | 0.3070 | 0.0100 | 1726 | 50 |
| 钾长花岗岩 | | | | | | | | | |
| LW3-1-1 | 429 | 436 | 0.98 | 0.1142 | 0.0101 | 0.0204 | 0.0004 | 130 | 3 |
| LW3-1-2 | 859 | 888 | 0.97 | 0.1227 | 0.0072 | 0.0196 | 0.0003 | 125 | 2 |
| LW3-1-4 | 463 | 457 | 1.01 | 0.1145 | 0.0101 | 0.0185 | 0.0004 | 118 | 3 |
| LW3-1-5 | 454 | 409 | 1.11 | 0.2316 | 0.0236 | 0.0203 | 0.0006 | 130 | 3 |
| LW3-1-6 | 225 | 287 | 0.78 | 0.1172 | 0.0116 | 0.0186 | 0.0004 | 119 | 3 |
| LW3-1-7 | 610 | 515 | 1.18 | 0.1161 | 0.0095 | 0.0185 | 0.0004 | 118 | 2 |
| LW3-1-8 | 246 | 318 | 0.77 | 0.1327 | 0.0130 | 0.0194 | 0.0004 | 124 | 3 |
| LW3-1-9 | 414 | 218 | 1.90 | 0.1852 | 0.0245 | 0.0203 | 0.0007 | 130 | 5 |
| LW3-1-10 | 294 | 322 | 0.91 | 0.1282 | 0.0122 | 0.0193 | 0.0004 | 123 | 3 |
| LW3-1-12 | 438 | 725 | 0.60 | 0.1188 | 0.0086 | 0.0192 | 0.0004 | 123 | 2 |
| LW3-1-13 | 241 | 408 | 0.59 | 0.1258 | 0.0107 | 0.0195 | 0.0005 | 124 | 3 |
| LW3-1-14 | 274 | 339 | 0.81 | 0.1466 | 0.0172 | 0.0197 | 0.0005 | 126 | 3 |
| LW3-1-15 | 256 | 306 | 0.84 | 0.1211 | 0.0115 | 0.0193 | 0.0005 | 123 | 3 |
| LW3-1-16 | 659 | 759 | 0.87 | 0.1056 | 0.0079 | 0.0192 | 0.0004 | 123 | 2 |
| LW3-1-17 | 468 | 637 | 0.73 | 0.1198 | 0.0104 | 0.0190 | 0.0003 | 122 | 2 |
| LW3-1-18 | 366 | 266 | 1.38 | 0.1573 | 0.0138 | 0.0187 | 0.0005 | 120 | 3 |
| LW3-1-20 | 155 | 161 | 0.96 | 0.1586 | 0.0211 | 0.0188 | 0.0005 | 120 | 3 |
| LW3-1-21 | 128 | 140 | 0.91 | 0.1644 | 0.0202 | 0.0190 | 0.0007 | 122 | 5 |
| LW3-1-22 | 776 | 795 | 0.98 | 0.1298 | 0.0074 | 0.0192 | 0.0004 | 122 | 3 |
| LW3-1-23 | 620 | 605 | 1.02 | 0.1290 | 0.0089 | 0.0193 | 0.0003 | 123 | 2 |
| LW3-1-24 | 513 | 525 | 0.98 | 0.1490 | 0.0123 | 0.0194 | 0.0004 | 124 | 2 |
| LW3-1-25 | 240 | 319 | 0.75 | 0.1496 | 0.0163 | 0.0197 | 0.0004 | 126 | 3 |
| LW3-1-26 | 475 | 531 | 0.90 | 0.1316 | 0.0094 | 0.0200 | 0.0004 | 128 | 2 |
| LW3-1-27 | 173 | 215 | 0.80 | 0.1683 | 0.0165 | 0.0186 | 0.0005 | 119 | 3 |
| LW3-1-28 | 661 | 738 | 0.90 | 0.1278 | 0.0086 | 0.0185 | 0.0003 | 118 | 2 |
| LW3-1-29 | 354 | 339 | 1.04 | 0.1382 | 0.0138 | 0.0189 | 0.0004 | 121 | 2 |
| LW3-1-30 | 359 | 486 | 0.74 | 0.1381 | 0.0107 | 0.0188 | 0.0004 | 120 | 2 |

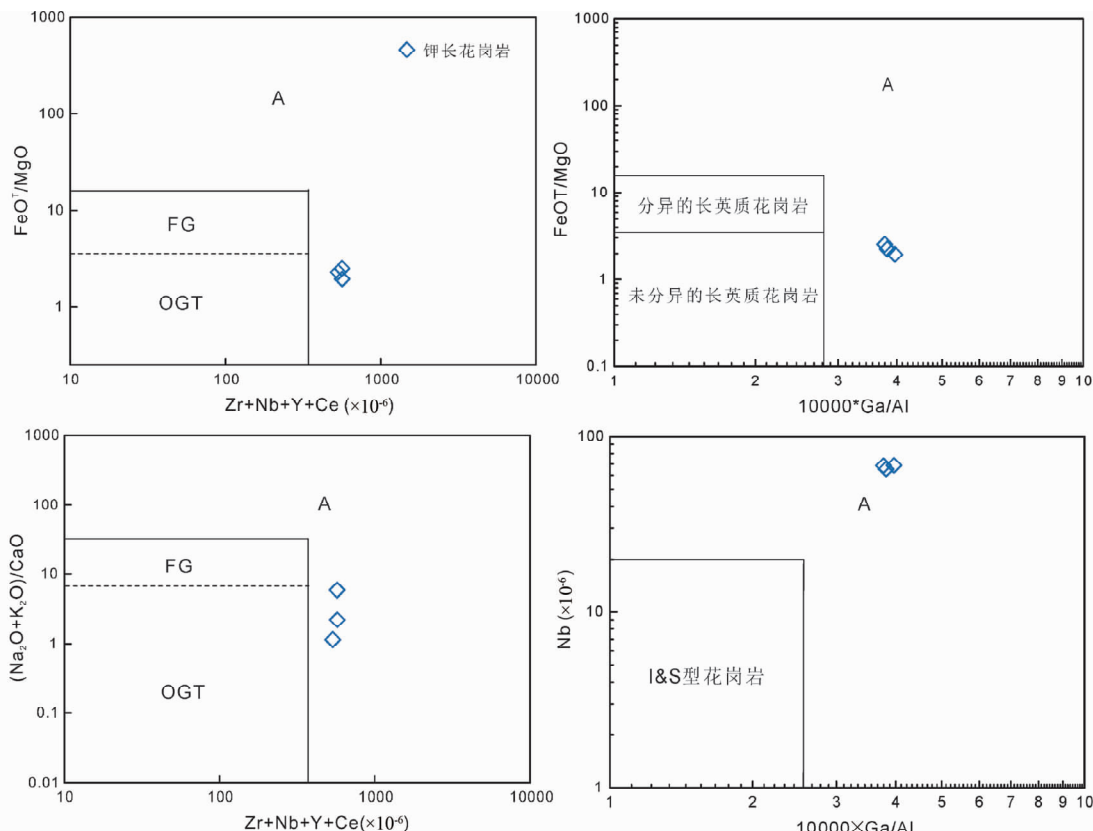


图7 李湾矿区岩体A型花岗岩判别图解(据 Whalen *et al.*, 1987)

Fig. 7 A-type granites discrimination diagram of Liwan intrusions (after Whalen *et al.*, 1987)

包裹体等地质现象也能看出(图3i)。玄武安山玢岩继承锆石2156 Ma的年龄值暗示了扬子板块东北缘长江中下游地区存在古元古代基底,古元古代基底参与了长江中下游中生代花岗质岩的形成,并产生了大量的斑岩型和矽卡岩型矿床(涂荫玖等, 2001; Gao *et al.*, 2001; Zheng *et al.*, 2006; Zhu *et al.*, 2014)。钾长花岗岩和闪长岩不同的结晶年龄说明李湾地区经历了不同的岩浆演化历史,由于闪长岩与本区矽卡岩紧密相关且本身也含铜钼矿(化),所以其年龄更接近铜多金属成矿的年龄,且与长江中下游地区A型花岗岩的形成时代相一致(125 ± 2 Ma; 范裕等, 2008; Wong *et al.*, 2009; Li *et al.*, 2011)。

4.3 锆石微量元素与 Hf 同位素

所有锆石微量元素测试数据见表4,Hf同位素分析结果见表5。

钾长花岗岩和闪长岩锆石稀土元素配分模式均显示典型的轻稀土亏损,重稀土富集,Ce正异常、Eu负异常的特征(图9a, b)。闪长岩锆石稀土总量(REE)范围为 598×10^{-6} ~ 2122×10^{-6} ,均值 1587×10^{-6} ;钾长花岗岩锆石稀土总量(REE)范围为 $746 \sim 2222 \times 10^{-6}$,均值 1343×10^{-6} ,说明两者的锆石稀土总量相似。闪长岩和钾长花岗岩锆石部分显示

较高的轻稀土富集特征,可能是在锆石分析时激光点位置打在了部分富轻稀土矿物(磷灰石)或包裹体上(Wang *et al.*, 2014)。通过晶格应力模型计算获得锆石的 $\text{Ce}^{4+}/\text{Ce}^{3+}$ 显示了闪长岩锆石具有较高的 $\text{Ce}^{4+}/\text{Ce}^{3+}$,平均值分别为497;而钾长花岗岩锆石 $\text{Ce}^{4+}/\text{Ce}^{3+}$ 偏低,平均值为246;钾长花岗岩锆石 $\text{Ce}^{4+}/\text{Ce}^{3+}$ 变化极大(10~3868),可能显示了锆石结晶时氧逸度变化大导致。闪长岩和钾长花岗岩锆石 Eu/Eu^* 均值为0.21;锆石Ti温度计算显示,两者的形成温度大体一致,闪长岩及钾长花岗岩的形成温度均值分别为:708°C及721°C。

钾长花岗岩岩浆锆石均具有均一的Hf同位素组成,锆石 $^{176}\text{Hf}/^{177}\text{Hf}$ 初始比值为 $0.28254 \sim 0.28267$,相应的 $\varepsilon_{\text{Hf}}(t)$ 为 $-6.7 \sim -2.1$,均值为 -4.7 ,二阶段模式年龄为 $1.12 \sim 1.36$ Ga,平均为 1.26 Ga(图9c)。李献华等(1991)统计前人数据,发现华南地壳幕式增长,主要有3期: 2.5 Ga或更早, 1.8 Ga, $1.2 \sim 1.4$ Ga。钾长花岗岩的源区对应晚期华南地壳的幕式增长,其锆石的二阶段Hf模式年龄与皖南地区出露的中元古代基底的年龄值相近, $\varepsilon_{\text{Hf}}(t)$ 说明李湾矿区侵入岩具有壳幔混合的岩浆岩源区的性质(图10),钾长花岗岩的初始岩浆可能属于皖南基底的部分熔融和地幔物质的混溶。

表 4 李湾矿区岩体锆石微量元素组成 ($\times 10^{-6}$)Table 4 Zircon trace element data for the Liwan intrusions ($\times 10^{-6}$)

| 测点号 | LW2-1-1 | LW2-1-2 | LW2-1-3 | LW2-1-4 | LW2-1-5 | LW2-1-10 | LW3-1-1 | LW3-1-2 | LW3-1-4 | LW3-1-5 | LW3-1-6 |
|-------------------|---------|---------|---------|---------|---------|----------|---------|---------|---------|---------|---------|
| P | 328.5 | 422.8 | 851.3 | 259.4 | 493.9 | 412.1 | 417.8 | 317.9 | 825.5 | 410.5 | 367.0 |
| Ti | 4.5 | 18.8 | 139.4 | 10.9 | 4.9 | 6.9 | 10.9 | 3.9 | 40.0 | 68.9 | 8.3 |
| Y | 2150 | 1660 | 1859 | 754.3 | 800.9 | 2127 | 1282 | 1666 | 2114 | 1233 | 1203 |
| Nb | 17.5 | 6.5 | 22.5 | 5.0 | 2.7 | 26.5 | 9.6 | 16.5 | 8.0 | 15.8 | 7.5 |
| La | 1.3 | 1.5 | 27.1 | 0.00 | 3.9 | 1.6 | 1.2 | 1.5 | 15.4 | 2.1 | 0.4 |
| Ce | 111.5 | 17.9 | 72.2 | 44.3 | 22.8 | 138.4 | 70.4 | 99.5 | 111.1 | 95.5 | 63.5 |
| Pr | 0.5 | 0.7 | 7.5 | 0.0 | 1.5 | 0.8 | 0.4 | 0.4 | 4.5 | 0.6 | 0.2 |
| Nd | 4.0 | 5.5 | 32.1 | 0.7 | 10.0 | 4.0 | 3.6 | 3.0 | 22.9 | 4.4 | 2.1 |
| Sm | 5.5 | 8.3 | 13.5 | 2.3 | 6.1 | 5.3 | 4.8 | 4.0 | 13.3 | 5.6 | 4.0 |
| Eu | 0.8 | 1.3 | 0.7 | 0.3 | 0.7 | 0.6 | 0.8 | 0.5 | 1.5 | 0.8 | 0.7 |
| Gd | 29.6 | 44.1 | 49.6 | 13.5 | 22.8 | 29.6 | 22.8 | 21.0 | 50.4 | 27.0 | 21.7 |
| Tb | 11.8 | 14.9 | 17.1 | 4.9 | 7.1 | 12.8 | 8.5 | 8.6 | 17.7 | 9.1 | 8.3 |
| Dy | 162.7 | 173.5 | 200.4 | 63.5 | 77.8 | 166.7 | 106.0 | 122.7 | 208.6 | 110.0 | 100.8 |
| Ho | 72.2 | 64.5 | 76.9 | 25.3 | 28.1 | 74.8 | 42.5 | 56.5 | 81.9 | 41.2 | 40.9 |
| Er | 393.0 | 281.0 | 339.0 | 121.6 | 121.2 | 384.9 | 203.0 | 315.2 | 379.2 | 196.2 | 191.6 |
| Tm | 97.3 | 56.0 | 69.9 | 27.0 | 25.1 | 93.3 | 46.7 | 80.4 | 83.4 | 44.3 | 42.4 |
| Yb | 1011 | 488.2 | 637.8 | 258.4 | 227.1 | 944.7 | 446.9 | 863.7 | 772.8 | 445.7 | 401.2 |
| Lu | 220.2 | 93.7 | 119.8 | 51.8 | 44.2 | 192.0 | 90.7 | 190.8 | 152.2 | 93.7 | 80.6 |
| Hf | 8511 | 7160 | 8844 | 7393 | 6772 | 8066 | 7095 | 8347 | 7487 | 6943 | 7495 |
| Ta | 4.2 | 3.0 | 7.4 | 2.1 | 1.3 | 6.1 | 3.2 | 4.2 | 3.1 | 3.4 | 3.0 |
| Pb | 22.7 | 13.8 | 27.2 | 3.9 | 7.3 | 26.5 | 12.2 | 23.4 | 11.8 | 12.6 | 7.0 |
| Th | 925.8 | 299.5 | 453.0 | 113.8 | 144.7 | 1148.8 | 428.9 | 859.1 | 463.0 | 453.9 | 224.9 |
| U | 919.2 | 555.2 | 1054.5 | 166.8 | 291.9 | 1061.1 | 436.1 | 887.5 | 457.4 | 409.0 | 287.1 |
| Zr | 369697 | 367932 | 376431 | 350319 | 348762 | 377623 | 351884 | 353529 | 358451 | 302476 | 358628 |
| Σ REE | 2122 | 1251 | 1664 | 613.7 | 598.3 | 2049 | 1048 | 1768 | 1915 | 1076 | 958.3 |
| LREE | 124.1 | 35.1 | 153.1 | 47.7 | 45.0 | 150.8 | 81.3 | 108.8 | 168.7 | 109.0 | 70.8 |
| HREE | 1998 | 1216 | 1510 | 566.0 | 553.3 | 1899 | 967.1 | 1659 | 1746 | 967.3 | 887.5 |
| Th/U | 1.0 | 0.5 | 0.4 | 0.7 | 0.5 | 1.1 | 1.0 | 1.0 | 1.0 | 1.1 | 0.8 |
| Ce^{4+}/Ce^{3+} | 983 | 32.1 | 66.3 | 575.6 | 37.2 | 1290 | 63.0 | 282 | 21.6 | 65.0 | 70.7 |
| Eu/Eu^* | 0.2 | 0.2 | 0.1 | 0.2 | 0.2 | 0.2 | 0.3 | 0.2 | 0.2 | 0.2 | 0.2 |
| T_{Zr} (°C) | 675 | 699 | 739 | 749 | 682 | 710 | 748 | 665 | 749 | 743 | 725 |

| 测点号 | LW3-1-7 | LW3-1-8 | LW3-1-9 | LW3-1-10 | LW3-1-12 | LW3-1-13 | LW3-1-14 | LW3-1-15 | LW3-1-16 | LW3-1-17 | LW3-1-18 |
|-------------------|---------|---------|---------|----------|----------|----------|----------|----------|----------|----------|----------|
| P | 431.4 | 2060.7 | 501.9 | 414.0 | 368.6 | 273.0 | 669.6 | 634.3 | 274.2 | 192.5 | 1493.0 |
| Ti | 9.6 | 10.8 | 40.0 | 6.9 | 30.6 | 5.4 | 11.8 | 9.6 | 5.1 | 4.2 | 19.1 |
| Y | 2555 | 1202 | 1694 | 1671 | 957.4 | 1146 | 1202 | 1259 | 1364 | 1226 | 2050 |
| Nb | 12.4 | 8.7 | 6.7 | 5.4 | 14.5 | 12.9 | 9.6 | 8.4 | 18.2 | 16.7 | 10.4 |
| La | 0.1 | 49.7 | 3.3 | 1.2 | 0.1 | 0.0 | 9.3 | 10.6 | 0.0 | 0.1 | 43.0 |
| Ce | 115.3 | 182.3 | 144.1 | 63.2 | 52.0 | 50.7 | 83.1 | 93.8 | 87.5 | 79.4 | 217.0 |
| Pr | 0.4 | 15.3 | 1.1 | 0.5 | 0.1 | 0.0 | 3.0 | 3.2 | 0.1 | 0.1 | 13.5 |
| Nd | 5.4 | 69.2 | 9.8 | 3.3 | 0.6 | 1.2 | 13.7 | 14.3 | 1.1 | 1.0 | 64.2 |
| Sm | 9.5 | 17.6 | 12.8 | 6.4 | 0.6 | 2.4 | 6.1 | 7.2 | 2.6 | 1.9 | 22.9 |
| Eu | 1.6 | 1.4 | 2.3 | 0.9 | 0.2 | 0.4 | 0.9 | 1.0 | 0.5 | 0.3 | 2.1 |
| Gd | 53.2 | 33.9 | 56.2 | 36.5 | 6.4 | 14.4 | 24.1 | 27.6 | 16.4 | 11.3 | 67.4 |
| Tb | 20.0 | 9.9 | 17.3 | 13.6 | 3.1 | 6.1 | 8.5 | 9.6 | 6.6 | 5.3 | 21.0 |
| Dy | 250.4 | 113.7 | 192.9 | 164.1 | 47.0 | 84.2 | 106.2 | 114.0 | 95.2 | 76.5 | 232.5 |
| Ho | 99.9 | 43.1 | 67.4 | 64.3 | 24.2 | 36.2 | 42.3 | 44.6 | 42.6 | 36.3 | 83.7 |
| Er | 467.9 | 197.1 | 281.9 | 296.4 | 156.0 | 186.2 | 199.6 | 206.0 | 231.1 | 209.2 | 352.9 |
| Tm | 100.4 | 43.1 | 56.5 | 63.4 | 45.0 | 44.8 | 43.9 | 44.5 | 57.2 | 54.6 | 69.8 |
| Yb | 921.2 | 404.0 | 498.5 | 578.1 | 537.6 | 455.1 | 418.8 | 416.2 | 596.7 | 593.8 | 603.8 |
| Lu | 177.4 | 79.7 | 94.4 | 111.4 | 131.5 | 96.2 | 82.8 | 80.4 | 130.5 | 129.9 | 113.9 |
| Hf | 7487 | 7491 | 6447 | 7708 | 8645 | 7938 | 7560 | 7547 | 8189 | 8442 | 6612 |
| Ta | 3.5 | 3.2 | 1.8 | 2.4 | 3.4 | 4.6 | 3.2 | 3.1 | 4.3 | 3.9 | 2.8 |
| Pb | 13.4 | 8.0 | 7.3 | 8.3 | 17.1 | 9.6 | 8.3 | 7.6 | 19.0 | 15.3 | 7.6 |
| Th | 610.4 | 246.2 | 414.1 | 293.9 | 437.7 | 240.9 | 274.0 | 255.8 | 658.7 | 467.8 | 365.9 |
| U | 515.2 | 318.2 | 217.9 | 321.9 | 725.5 | 407.6 | 338.9 | 305.6 | 759.4 | 637.1 | 265.7 |
| Zr | 353584 | 354100 | 353012 | 353775 | 358038 | 355293 | 357488 | 361335 | 363977 | 359522 | 350643 |
| Σ REE | 2223 | 1260 | 1438 | 1403 | 1004 | 977.8 | 1042 | 1073 | 1268 | 1199 | 1908 |
| LREE | 132.2 | 335.5 | 173.4 | 75.4 | 53.5 | 54.7 | 116.0 | 130.1 | 91.7 | 82.6 | 362.7 |
| HREE | 2090 | 924.7 | 1265 | 1328 | 950.7 | 923.1 | 926.2 | 942.9 | 1176 | 1117 | 1545 |
| Th/U | 1.2 | 0.8 | 1.9 | 0.9 | 0.6 | 0.6 | 0.8 | 0.8 | 0.87 | 0.73 | 1.38 |
| Ce^{4+}/Ce^{3+} | 50.0 | 11.0 | 18.0 | 36.9 | 3868 | 192.5 | 42.9 | 33.6 | 398 | 640 | 10.3 |
| Eu/Eu^* | 0.2 | 0.2 | 0.3 | 0.2 | 0.3 | 0.2 | 0.2 | 0.2 | 0.22 | 0.16 | 0.16 |
| T_{Zr} (°C) | 738 | 747 | 748 | 710 | 749 | 690 | 745 | 737 | 686 | 670 | 750 |

续表 4

Continued Table 4

| 测点号 | LW3-1-20 | LW3-1-21 | LW3-1-22 | LW3-1-23 | LW3-1-24 | LW3-1-25 | LW3-1-26 | LW3-1-27 | LW3-1-28 | LW3-1-29 | LW3-1-30 |
|-------------------|----------|----------|----------|----------|----------|----------|----------|----------|----------|----------|----------|
| P | 296.2 | 342.0 | 679.7 | 325.6 | 253.3 | 319.5 | 541.5 | 320.3 | 662.3 | 600.5 | 1631.2 |
| Ti | 15.2 | 15.8 | 4.2 | 5.7 | 5.1 | 7.7 | 6.9 | 11.6 | 4.4 | 13.8 | 36.4 |
| Y | 964.8 | 958.1 | 2216 | 2188 | 1834 | 1141 | 1607 | 1012 | 1672 | 1566 | 1014 |
| Nb | 3.6 | 3.9 | 15.1 | 8.6 | 7.7 | 8.2 | 11.1 | 5.3 | 13.2 | 6.7 | 11.2 |
| La | 0.0 | 0.0 | 10.9 | 0.0 | 0.1 | 0.0 | 5.0 | 0.0 | 21.1 | 11.7 | 60.7 |
| Ce | 51.7 | 54.8 | 118.1 | 77.9 | 70.5 | 57.9 | 85.9 | 59.2 | 116.2 | 100.6 | 171.6 |
| Pr | 0.2 | 0.1 | 2.6 | 0.3 | 0.2 | 0.1 | 1.2 | 0.1 | 3.8 | 3.2 | 12.0 |
| Nd | 2.1 | 2.0 | 11.9 | 5.1 | 2.9 | 1.4 | 7.3 | 1.6 | 14.8 | 16.7 | 42.4 |
| Sm | 4.1 | 3.8 | 6.2 | 8.0 | 5.4 | 3.4 | 6.6 | 3.4 | 5.3 | 9.0 | 8.5 |
| Eu | 0.8 | 0.7 | 0.6 | 1.2 | 0.7 | 0.8 | 1.0 | 0.6 | 0.6 | 1.5 | 0.7 |
| Gd | 21.9 | 20.6 | 31.4 | 40.7 | 28.9 | 20.0 | 31.9 | 19.6 | 22.2 | 39.4 | 18.6 |
| Tb | 7.1 | 7.2 | 12.1 | 15.4 | 11.1 | 7.6 | 11.9 | 7.2 | 8.8 | 13.1 | 6.1 |
| Dy | 86.0 | 85.5 | 167.5 | 194.3 | 148.0 | 95.3 | 149.9 | 87.9 | 120.8 | 155.6 | 74.7 |
| Ho | 32.5 | 32.6 | 74.5 | 80.8 | 63.5 | 38.3 | 60.1 | 35.0 | 55.3 | 58.0 | 31.5 |
| Er | 150.5 | 146.7 | 397.4 | 396.6 | 326.6 | 184.7 | 281.4 | 161.4 | 304.2 | 265.0 | 161.1 |
| Tm | 32.8 | 32.0 | 94.9 | 91.5 | 77.5 | 41.3 | 63.0 | 35.2 | 78.7 | 57.2 | 38.8 |
| Yb | 311.6 | 300.8 | 962.3 | 890.1 | 773.9 | 397.6 | 602.3 | 340.2 | 842.0 | 542.6 | 401.8 |
| Lu | 63.2 | 59.7 | 200.0 | 184.2 | 163.3 | 81.2 | 119.7 | 67.1 | 185.4 | 108.7 | 85.8 |
| Hf | 6930 | 7015 | 7989 | 7775 | 8162 | 7488 | 7665 | 7356 | 8214 | 7157 | 7774 |
| Ta | 1.5 | 1.5 | 3.6 | 2.8 | 2.4 | 2.8 | 3.8 | 2.3 | 3.3 | 1.9 | 3.4 |
| Pb | 4.2 | 3.5 | 20.4 | 15.5 | 13.6 | 8.0 | 14.1 | 5.2 | 18.4 | 9.0 | 12.2 |
| Th | 155.1 | 127.7 | 776.4 | 619.6 | 512.9 | 240.3 | 475.5 | 173.4 | 660.7 | 354.0 | 358.7 |
| U | 161.1 | 139.8 | 795.1 | 605.0 | 524.9 | 319.2 | 530.8 | 215.5 | 737.6 | 339.5 | 485.7 |
| Zr | 345455 | 352797 | 338712 | 351195 | 345827 | 347348 | 348600 | 346701 | 344295 | 346049 | 320241 |
| Σ REE | 764.6 | 746.7 | 2090 | 1986 | 1673 | 929.6 | 1427 | 818.3 | 1779 | 1382 | 1114 |
| LREE | 58.9 | 61.5 | 150.2 | 92.5 | 79.9 | 63.6 | 107.0 | 64.9 | 161.9 | 142.7 | 295.9 |
| HREE | 705.7 | 685.2 | 1940 | 1894 | 1593 | 866.0 | 1320 | 753.4 | 1617 | 1240 | 818.3 |
| Th/U | 0.96 | 0.91 | 0.98 | 1.02 | 0.98 | 0.75 | 0.90 | 0.80 | 0.90 | 1.04 | 0.74 |
| Ce^{4+}/Ce^{3+} | 43.7 | 50.1 | 143 | 51.1 | 89.3 | 90.1 | 52.4 | 76.4 | 182 | 30.2 | 50.7 |
| Eu/Eu^* | 0.27 | 0.25 | 0.12 | 0.21 | 0.18 | 0.28 | 0.21 | 0.21 | 0.18 | 0.25 | 0.17 |
| T_{Zr} (°C) | 749 | 743 | 671 | 694 | 686 | 719 | 710 | 744 | 674 | 750 | 748 |

表 5 李湾矿区岩体锆石 Hf 同位素组成

Table 5 Zircon Hf isotope data for the Liwan intrusions

| 测点号 | t_{Ma} | $^{176}\text{Yb}/^{177}\text{Hf}$ | $^{176}\text{Lu}/^{177}\text{Hf}$ | $^{176}\text{Hf}/^{177}\text{Hf}$ | 2σ | $\varepsilon_{\text{Hf}}(0)$ | $\varepsilon_{\text{Hf}}(t)$ | t_{DMI} (Ma) | t_{DMC} (Ma) |
|----------|----------|-----------------------------------|-----------------------------------|-----------------------------------|-----------|------------------------------|------------------------------|-------------------------|-------------------------|
| LW3-1-01 | | 0.066657 | 0.002898 | 0.282582 | 0.000006 | -7.7 | -5.3 | 1072 | 1281 |
| LW3-1-02 | | 0.033121 | 0.001261 | 0.282567 | 0.000008 | -8.3 | -5.7 | 1047 | 1303 |
| LW3-1-03 | | 0.050753 | 0.00205 | 0.282609 | 0.000006 | -6.8 | -4.2 | 1008 | 1229 |
| LW3-1-04 | | 0.037497 | 0.001407 | 0.282567 | 0.000008 | -8.3 | -5.7 | 1051 | 1303 |
| LW3-1-05 | | 0.037199 | 0.001423 | 0.282617 | 0.000006 | -6.5 | -3.9 | 980 | 1212 |
| LW3-1-06 | | 0.048465 | 0.001941 | 0.282614 | 0.000008 | -6.6 | -4.1 | 998 | 1220 |
| LW3-1-07 | | 0.058113 | 0.002199 | 0.282539 | 0.000009 | -9.2 | -6.7 | 1114 | 1356 |
| LW3-1-08 | 122 | 0.024953 | 0.000972 | 0.282583 | 0.000007 | -7.7 | -5.1 | 1016 | 1272 |
| LW3-1-09 | | 0.052975 | 0.001994 | 0.28267 | 0.000007 | -4.6 | -2.1 | 919 | 1119 |
| LW3-1-10 | | 0.035045 | 0.001334 | 0.282628 | 0.000007 | -6.1 | -3.5 | 963 | 1193 |
| LW3-1-11 | | 0.030748 | 0.001263 | 0.282556 | 0.000008 | -8.6 | -6.1 | 1062 | 1322 |
| LW3-1-12 | | 0.036656 | 0.001445 | 0.282618 | 0.000006 | -6.5 | -3.9 | 980 | 1212 |
| LW3-1-13 | | 0.078681 | 0.00282 | 0.28262 | 0.000009 | -6.4 | -3.9 | 1014 | 1212 |
| LW3-1-14 | | 0.061466 | 0.002312 | 0.282579 | 0.000008 | -7.8 | -5.3 | 1060 | 1285 |
| LW3-1-15 | | 0.066318 | 0.002371 | 0.282602 | 0.000008 | -7.0 | -4.5 | 1028 | 1243 |
| LW3-1-16 | | 0.053975 | 0.002055 | 0.282558 | 0.000007 | -8.6 | -6.1 | 1082 | 1322 |

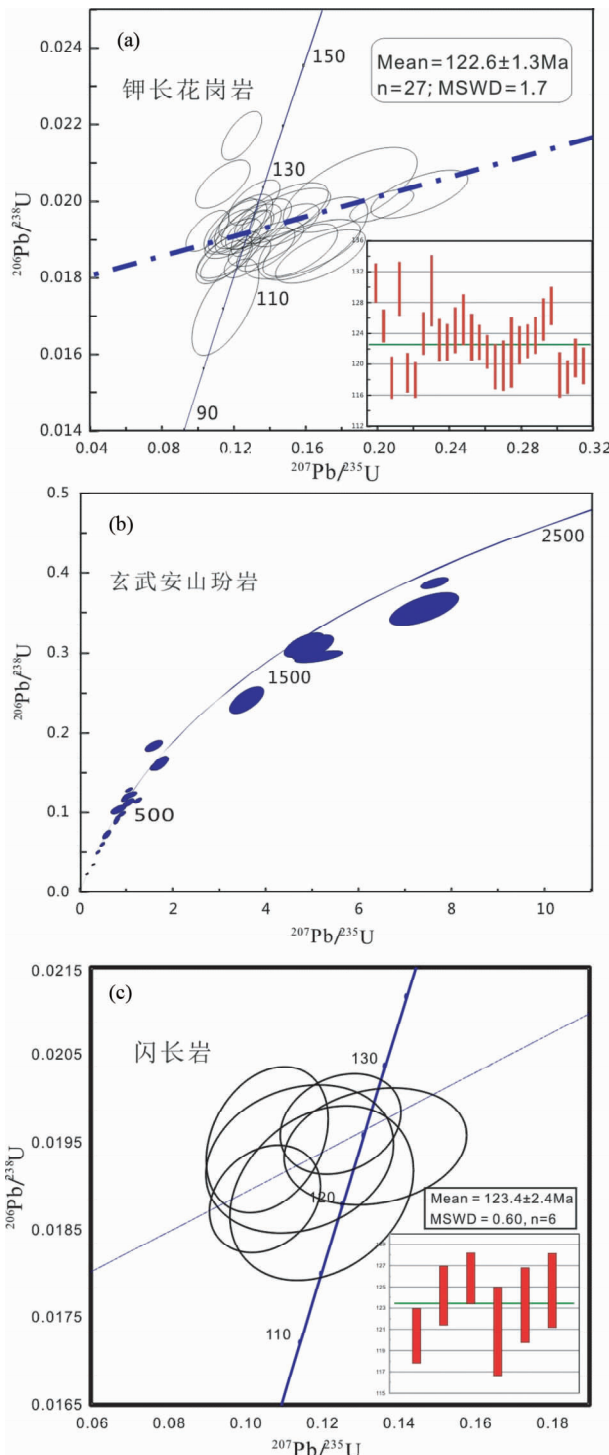


图 8 李湾矿区岩体锆石年龄图解

Fig. 8 Zircon concordia diagrams of zircon from Liwan intrusions
Ellipse dimensions are 1σ

5 讨论

5.1 岩石成因

研究表明皖南地区 A 型花岗岩初始 ($^{87}\text{Sr}/^{86}\text{Sr}$) 约为

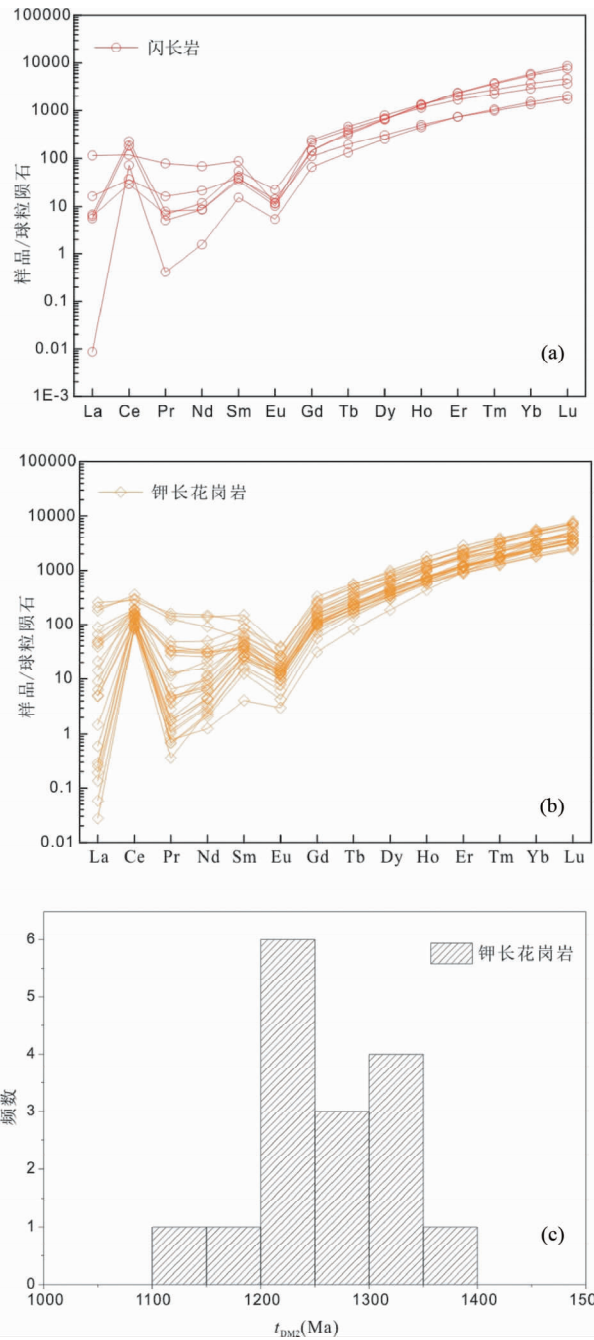


图 9 李湾矿区岩体锆石稀土配分图(a、b, 标准化值据 Sun and McDonough, 1989) 及钾长花岗岩二阶模式年龄图解(c)

Fig. 9 Chondrite-normalized REE patterns of zircons from Liwan intrusions (a, b, normalization values from Sun and McDonough, 1989) and two second model age plot of K-feldspar granites (c)

$0.707, \varepsilon_{\text{Nd}}(t)$ 为 $-4.2 \sim -7.0$, Nd 模式年龄为 $1.2 \sim 1.5\text{ Ga}$, 这些岩体可能来源于中元古代的物源区的部分熔融(张舒等, 2009)。李湾矿区 A 型花岗岩样品与皖南地区其它 A 型花岗岩相比具有相似的地球化学特征, 同时其锆石 $\varepsilon_{\text{Hf}}(t)$ 为 $-6.7 \sim -2.1$, 均值为 -4.7 , 二阶段模式年龄平均为

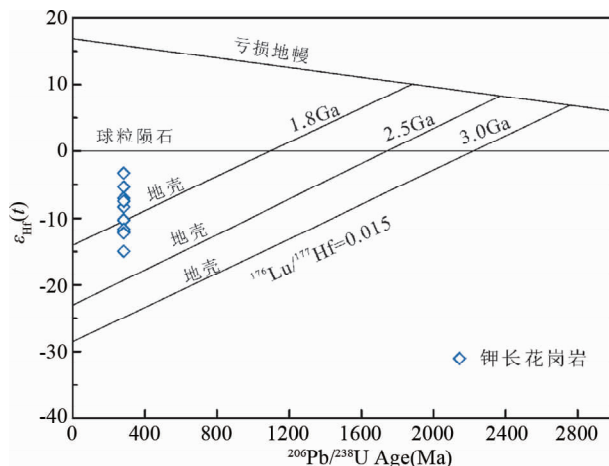


图 10 岩体 U-Pb 年龄与 Hf 图解

Fig. 10 U-Pb age vs. Hf diagram of Liwan intrusions

1.26Ga,这些特征表明,其成岩可能与皖南 A型花岗岩类似,具有地幔物质与皖南基底古老变质岩混合的源区特征。

在锆石微量元素变异图解中(图 11),总体上,钾长花岗岩及闪长岩中锆石微量元素具有一定的相关关系,暗示成因上联系。闪长岩锆石 $\text{Ce}^{4+}/\text{Ce}^{3+}$ 比值和 Eu/Eu^* 分别为 7.28~814(均值 327)和 0.08~0.75(均值 0.35);钾长花岗岩则为 10.3~3868(均值 247)和 0.12~0.28(均值 0.21)。利用锆石原位微量元素特征区分出大陆地壳和大洋地壳锆石。

在 Yb-U 图解中(图 12),所有锆石样品的 Yb 和 U 含量比较集中,具有正相关关系,大都落在镁质锆石区域内,并主要集中在镁质、陆壳和洋壳锆石相重叠区域,暗示本区侵入岩的源区存在岩浆混合的可能性。本区侵入岩中锆石微量元素较明显的相关关系反映其岩浆过程主要为共存结晶作用,并在锆石结晶演化过程中得以记录(Gagnevin *et al.*, 2010)。值得注意的是,随着 Yb 和 U 含量的增加,两个样品成分点均向洋壳锆石区域偏移,暗示洋壳成分在岩浆源区占有重要的支配。

研究表明随着 Ti 含量减少或锆石温度降低,大洋地壳锆石中 Hf 和大多数微量元素含量(如,U,Th,Y,P 和 HREE)明显富集,李湾样品具有这个特征。从锆石 $\text{Ce}^{4+}/\text{Ce}^{3+}$ 和 Eu 异常特征看,显示较高的氧逸度特征,有利于铜多金属成矿(Sun *et al.*, 2004, 2011; Ling *et al.*, 2009)。研究表明,俯冲带具有比板内更高的氧逸度特征(Sun *et al.*, 2004, 2010, 2011; Ling *et al.*, 2009)。该区岩浆岩锆石氧逸度特征进一步证明该地区可能先是经历了太平洋俯冲,而后在板块后撤过程中保留了部分俯冲的信息。其闪长岩最有可能来源于残留的俯冲洋壳部分熔融,并在其上升过程中与富集地幔发生相互作用。同时氧逸度还可以作为一个经验性的指标来区分成矿岩体与不成矿岩体,该区侵入岩具有较高的氧逸度,可能暗示了其具有较大的成矿潜力。

长江中下游 A型花岗岩的初始 Sr-Nd 同位素组成,明显

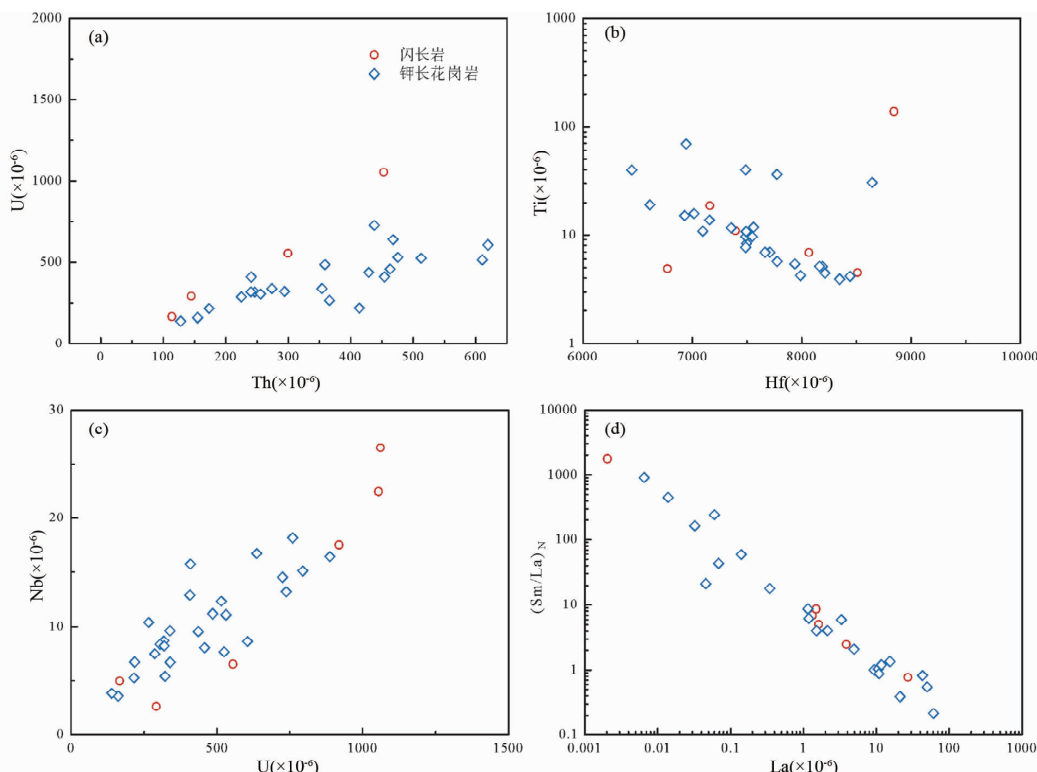


图 11 锆石微量元素地球化学变异图解

Fig. 11 Geochemical variation diagrams of zircon from the Liwan intrusive rocks

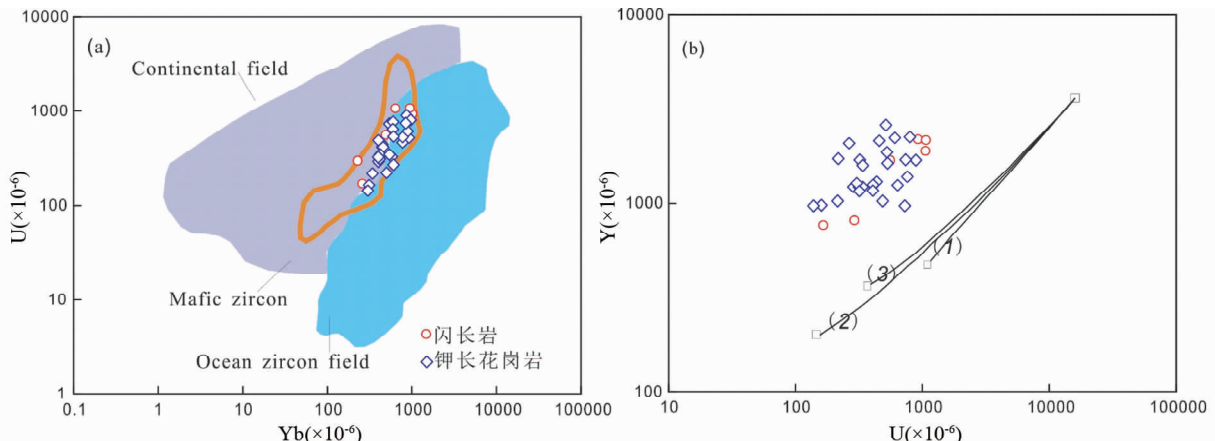


图 12 岩浆岩锆石 Yb-U (a) 及 U-Y (b) 图解

(a) 中陆壳、镁质和洋壳锆石区域引自数据 Grimes *et al.* (2009); (b) 中(1)、(2)和(3)曲线代表了混合模式, 来源于 Langmuir *et al.* (1978), 一个富 U-Y 锆石代表长英质端元, 三个贫 U-Y 锆石代表镁质端元

Fig. 12 Yb-U (a) and Th-Y (b) diagrams of zircon

(a) continental, mafic and ocean zircon field are after Grimes *et al.* (2009); (b) (1), (2) and (3) mixing models following Langmuir *et al.* (1978) using one U-Y-rich zircon to represent the felsic end-member and three U-Y-poor zircons to represent mafic end-members

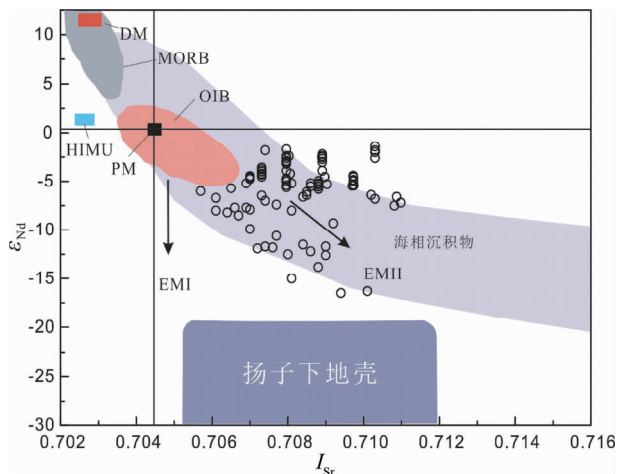


图 13 长江中下游 A 型花岗岩 Nd-Sr 图解

数据来源: MORB 和海相沉积物 (Hofmann, 2003), 扬子板块下地壳 (Chen and Jahn, 1998; Xing *et al.*, 1994), 长江中下游地区 A 型花岗岩 (Yang *et al.*, 2012; Jiang *et al.*, 2005, 2011; 张舒等, 2009; 薛怀民等, 2009; Chen *et al.*, 2001)

Fig. 13 Nd-Sr isotopic components diagram for the A-type granites in the LYRB

Data source: MORB and marine sediments (Hofmann, 2003); the lower crust of the Yangtze blocks (Chen and Jahn, 1998; Xing *et al.*, 1994); LYRB A-type granites (Yang *et al.*, 2012; Jiang *et al.*, 2005, 2011; Zhang *et al.*, 2009; Xue *et al.*, 2009; Chen *et al.*, 2001)

不同于扬子下地壳组成, 表明板块熔体遭受富集地幔成分的混染作用 (图 13, Ling *et al.*, 2009, 2011)。其趋向于 EM II 端元, 表明岩浆源区有俯冲沉积物加入 (Liu *et al.*, 2010b) (图 13)。然而, 沉积物通常 Cu 含量低, 因此不可能是李湾铜矿床的主要来源。鄂东、九瑞、安庆-贵池以及铜陵地区,

与铜矿床相关的含矿岩体侵位时间早于 135 Ma, $\varepsilon_{\text{Hf}}(t)$ 随着侵位时间变晚 $\varepsilon_{\text{Hf}}(t)$ 减小 (Ding *et al.*, 2006; Li *et al.*, 2008; 刘园园等, 2009; Wu *et al.*, 2012; Yang and Zhang, 2012)。这种变化趋势不能通过 Hf 的储存演化来解释, 而更可能是壳幔混染的部分熔融形成的。早期, 深部地壳物质拆沉并交代地幔物质, 随着时间推移, 更多的浅部地壳物质加入, 从而造成了越老的斑岩具有更高的 $\varepsilon_{\text{Hf}}(t)$ 值。相对九瑞、鄂东、铜陵地区, 李湾矿区岩体具有高的 $\varepsilon_{\text{Hf}}(t)$ 和老的年龄值, 说明在岩石形成过程中壳幔混染, 使得李湾铜矿床更多的富集 Cu。

综上所述, 这些明显的地球化学特征表明李湾和长江中下游地区 A 型花岗岩起源于有限俯冲沉积物贡献的俯冲洋壳部分熔融, 其上升过程中与富集地幔发生相互作用, 同时混染了古元古代基底物质。因此, 李湾地区钾长花岗岩是陆壳部分熔融与地幔混溶的结果, 而闪长岩可能是板块后撤过程中洋壳与地幔物质的混合。

5.2 构造及成矿意义

在构造环境判别图解中 (图 14), 闪长岩岩体都落在火山弧花岗岩范围内, 钾长花岗岩落在板内花岗岩范围, 玄武安山玢岩落在火山弧花岗岩范围内, 结合区域地质背景, 我们认为闪长岩成因是残留的洋壳部分熔融与地幔混合的产物, 而钾长花岗岩为陆壳部分熔融与地幔的混合的产物, 两者同位于板块后撤过程中的拉张背景中, 是地幔物质与不同地质体的混溶结果。闪长岩 ($\text{Al}_2\text{O}_3 + \text{Fe}_2\text{O}_3 + \text{MgO} + \text{TiO}_2$) 含量为 28.15% ~ 31.36%, $\text{Al}_2\text{O}_3 / (\text{Fe}_2\text{O}_3 + \text{MgO} + \text{TiO}_2)$ 比值变化在 1.05 ~ 1.54, 暗示熔体处在一个相对低压的环境。因此, 总体上李湾矿区的侵入岩形成于早白垩世高温-低压的板块俯冲后撤拉张的环境。富水的闪长岩与铜多金属成

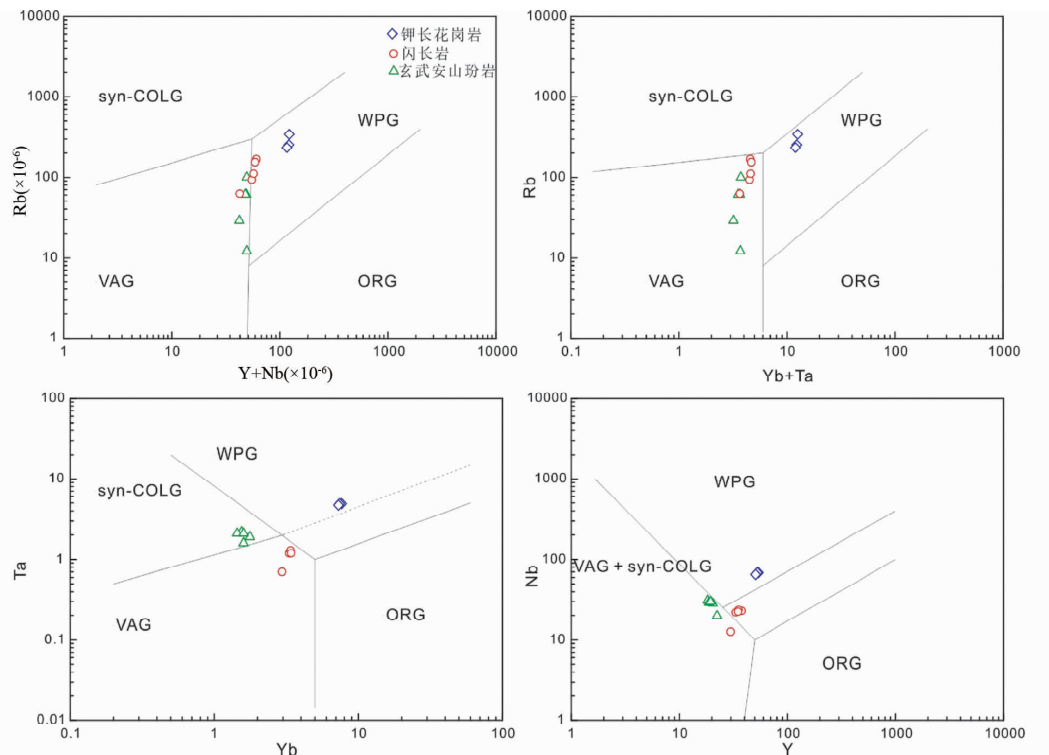


图 14 李湾矿区岩体构造判别图解(据 Pearce *et al.*, 1984)

WPG-板内花岗岩;ORG-洋中脊花岗岩;VAG-岛弧花岗岩;syn-COLG-同碰撞花岗岩

Fig. 14 Diagrams of tectonic environment for Liwan intrusive rocks (after Pearce *et al.*, 1984)

矿直接相关,而稍后的钾长花岗岩侵位则为本地区成矿提供了后期热动力,使成矿元素更加富集。

Mao *et al.* (2006) 认为长江中下游矿集区铜、金矿床的形成可能与古太平洋板块或依泽纳吉板块向欧亚大陆俯冲有关; Ling *et al.* (2009, 2011) 研究认为长江中下游成矿带中金属矿床的分布与太平洋和依泽纳吉板块之间的洋脊俯冲有关。李湾矿区侵入岩锆石微量元素显示具有高的 Ce 正异常特征,暗示岩浆形成于氧化环境。俯冲板片残留的洋壳部分熔融产生具有高氧逸度的熔体。地幔楔熔融时,Cu、Au 等趋向集中在硫化物熔体中,只有当地幔熔融源区呈现高氧化态时,S 元素才能更好地进入硅酸盐熔体,此时,Cu、Au 等成矿元素才能富集于硅酸盐熔体中。因此,本地区经历了 140 ± 5 Ma 的板块俯冲,在随后约 20 Myr 前后太平洋板块后撤过程中,先期俯冲的残留洋壳部分熔融为铜多金属成矿提供了物质来源。

6 结论

李湾矿区侵入岩锆石 U-Pb 年代学研究表明其闪长岩形成于 123.4 ± 2.4 Ma, 钾长花岗岩形成于 122.6 ± 1.3 Ma, 作为矽卡岩型铜多金属矿床,其成矿应接近或略晚于闪长岩的成岩年龄,因此其成岩成矿与长江中下游地区 125 Ma 左右的 A 型花岗岩岩浆活动及成矿时间大体一致。

李湾矽卡岩型铜多金属矿床与闪长岩密切相关,闪长岩全程参与了成矿,而随后的钾长花岗岩侵位为本区成矿提供了后续热动力(热源)。闪长岩可能是板块后撤过程中残留洋壳与地幔的混溶,而钾长花岗岩则是陆壳部分熔融与地幔混溶的结果,两者统一形成于太平洋板块在 125 Ma 左右俯冲后撤过程中造成的拉张背景环境中。

李湾矿区岩体继承锆石 2156 Ma 代表了基底岩石年龄,不仅证明了扬子板块东北缘存在古元古代基底物质,同时暗示了有古元古代基底的物质参与了本区深部物质的循环,最终形成壳幔混合型岩体,在与奥陶系石灰岩接触部位产生了矽卡岩型铜多金属矿床。

致谢 本文在成文过程中得到了邓江洪、汪方跃等博士的帮助;两位匿名审稿人给予了很好的指导和建议;在此一并致以衷心的感谢。

References

- Blichert TJ and Albarede F. 1997. The Lu-Hf isotope geochemistry of chondrites and the evolution of the mantle-crust system. *Earth and Planetary Science Letters*, 148(1-2): 243-258
- Chang YF, Liu XP and Wu YC. 1991. The Copper-Iron Belt of the Lower-Middle Research of the Changjiang River. Beijing: Geological Publishing House (in Chinese)
- Chen JF and Jahn BM. 1998. Crustal evolution of southeastern China:

- Nd and Sr isotopic evidence. *Tectonophysics*, 284(1–2): 101–133
- Chen JF, Yan J, Xie Z, Xu X and Xing F. 2001. Nd and Sr isotopic compositions of igneous rocks from the Lower Yangtze Region in eastern China: Constraints on sources. *Physics and Chemistry of the Earth*, 26(9–10): 719–731
- Chu NC, Taylor RN, Chavagnac V, Nesbitt RW, Boella RM, Milton JA, German CR, Bayon G and Burton K. 2001. Hf isotope ratio analysis using multi-collector inductively coupled plasma mass spectrometry: An evaluation of isobaric interference corrections. *Journal of Analytical Atomic Spectrometry*, 17(12): 1567–1574
- De Biévre P and Taylor PDP. 1993. Table of the isotopic compositions of the elements. *International Journal of Mass Spectrometry and Ion Processes*, 123(2): 149–166
- Deng J, Wang QF, Xiao CH, Yang LQ, Liu H, Gong QJ and Zhang J. 2011. Tectonic-magmatic-metallogenic system, Tongling ore cluster region, Anhui Province, China. *International Geology Review*, 53(5–6): 449–476
- Ding X, Jiang SY, Zhao KD, Nakamura E, Kobayashi K, Ni P, Gu LX and Jiang YH. 2006. In-situ U-Pb SIMS dating and trace element (EMPA) composition of zircon from a granodiorite porphyry in the Wushan copper deposit, China. *Mineralogy and Petrology*, 86: 29–44
- Dong S. 2006. Regional geochemical characteristics of Guichi area in Anhui Province and their ore-prospecting significance. *Geochemical and Geochemical Exploration*, 30(3): 215–223 (in Chinese with English abstract)
- Duan LA, Yang XY, Wang FY, Deng JH and Sun WD. 2012. Geochemistry and zircon U-Pb age of ore-bearing porphyry in the Paodaoling gold deposit in Guichi, Middle-Lower Yangtze metallogenic belt. *Acta Petrologica Sinica*, 28(10): 3241–3254 (in Chinese with English abstract)
- Duan LA, Yang XY, Liu XM and Sun WD. 2013. Discovery of gold deposit in the Silurian System in Suijidian, Tongling ore cluster region: Its significance. *Geotectonica et Metallogenesis*, 37(2): 333–339 (in Chinese with English abstract)
- Duan LA, Yang XY and Wang FY. 2014. Characteristics and prospects of Paodaoling large porphyry gold deposit in the Middle-Lower Yangtze River metallogenic belt. *Journal of Earth Sciences and Environment*, 36(1): 161–170 (in Chinese with English abstract)
- Fan Y, Zhou TF, Yuan F, Qian CC, Lu SM and Cooke D. 2008. LA-ICP-MS zircon U-Pb ages of the A-type granites in the Lu-Zong (Lujiang-Zongyang) area and their geological significances. *Acta Petrologica Sinica*, 24(8): 1715–1724 (in Chinese with English abstract)
- Gagnevin D, Daly JS and Kronz A. 2010. Zircon texture and chemical composition as a guide to magmatic processes and mixing in a granitic environment and coeval volcanic system. *Contributions to Mineralogy and Petrology*, 159(4): 579–596
- Gao S, Qiu YM, Ling WL, McNaughton NJ and Groves DI. 2001. Single zircon U-Pb dating of the Kongling high-grade metamorphic terrain: Evidence for >3.2 Ga old continental crust in the Yangtze craton. *Science in China (Series D)*, 44(4): 326–335
- Griffin WL, Pearson NJ, Belousova E, Jackson SE, van Achterbergh E, O'Reilly SY and Shee SR. 2000. The Hf isotope composition of cratonic mantle: LAM-MC-ICPMS analysis of zircon megacrysts in kimberlites. *Geochimica et Cosmochimica Acta*, 64(1): 133–147
- Griffin WL, Wang X, Jackson SE, Pearson NJ, O'Reilly SY, Xu XS and Zhou XM. 2002. Zircon chemistry and magma mixing, SE China: In-situ analysis of Hf isotopes, Tonglu and Pingtan igneous complexes. *Lithos*, 61(3–4): 237–269
- Grimes CB, John BE, Cheadle MJ, Mazdab FL, Wooden JL, Swapp S and Schwartz JJ. 2009. On the occurrence, trace element geochemistry, and crystallization history of zircon from in situ ocean lithosphere. *Contributions to Mineralogy and Petrology*, 158(6): 757–783
- Hofmann AW. 2003. Sampling mantle heterogeneity through oceanic basalts: Isotopes and trace elements. In: Carlson RW (ed.). The Mantle and Core. Treatise on Geochemistry. Oxford: Elsevier-Pergamon, 61–101
- Hoskin PWO. 2000. Patterns of chaos: Fractal statistics and the oscillatory chemistry of zircon. *Geochimica et Cosmochimica Acta*, 64(11): 1905–1923
- Jiang YH, Ling HF, Jiang SY, Fan HH, Shen WZ and Ni P. 2005. Petrogenesis of a Late Jurassic peraluminous volcanic complex and its high-Mg, potassic, quenched enclaves at Xiangshan, Southeast China. *Journal of Petrology*, 46(6): 1121–1154
- Jiang YH, Zhao P, Zhou Q, Liao SY and Jin GD. 2011. Petrogenesis and tectonic implications of Early Cretaceous S- and A-type granites in the northwest of the Gan-Hang rift, SE China. *Lithos*, 121(1–4): 55–73
- Langmuir CH, Vocke RDJR and Hanson GN. 1978. A general mixing equation with applications to Icelandic basalts. *Earth and Planetary Science Letters*, 37(3): 380–392
- Le Bas MJ, LeMaitre RW, Streckeisen A and Zanettin B. 1986. A chemical classification of volcanic rocks based on the total alkali-silica diagram. *Journal of Petrology*, 27(3): 745–750
- Li H, Zhang H, Ling MX, Wang FY, Ding X, Zhou JB, Yang XY, Tu XL and Sun WD. 2011. Geochemical and zircon U-Pb study of the Huangmeijian A-type granite: Implications for geological evolution of the Lower Yangtze River belt. *International Geology Review*, 53(5–6): 499–525
- Li H, Ling MX, Li CY, Zhang H, Ding X, Yang XY, Fan WM, Li YL and Sun WD. 2012. A-type granite belts of two chemical subgroups in central eastern China: Indication of ridge subduction. *Lithos*, 150: 26–36
- Li JW, Zhao XF, Zhou MF, Vasconcelos P, Ma CQ, Deng XD, Sérgio de Souza Z, Zhao YX and Wu G. 2008. Origin of the Tongshankou porphyry-skarn Cu-Mo deposit, eastern Yangtze craton, eastern China: Geochronological, geochemical, and Sr-Nd-Hf isotopic constraints. *Mineralium Deposita*, 43(3): 315–336
- Li JW, Zhao XF, Zhou MF, Ma CQ, de Souza ZS and Vasconcelos P. 2009. Late Mesozoic magmatism from the Daye region, eastern China: U-Pb ages, petrogenesis, and geodynamic implications. *Contributions to Mineralogy and Petrology*, 157(3): 383–409
- Li XH, Zhao ZH, Gui XT and Yu JS. 1991. Sm-Nd isotopic and zircon U-Pb constraints on the age of formation of the Precambrian crust in Southeast China. *Geochimica*, 20(3): 255–264 (in Chinese with English abstract)
- Li XH, Long WG, Li QL, Liu Y, Zheng YF, Yang YH, Chamberlain KR, Wan DF, Guo CH, Wang XC and Tao H. 2010. Penglai zircon megacrysts: A potential new working reference material for microbeam determination of Hf-O isotopes and U-Pb age. *Geostandards and Geoanalytical Research*, 34(2): 117–134
- Ling MX, Wang FY, Ding X, Yang YH, Zhou JB, Zartman RE, Yang XY and Sun WD. 2009. Cretaceous ridge subduction along the Lower Yangtze River Belt, eastern China. *Economic Geology*, 104(2): 303–321
- Ling MX, Wang FY, Ding X, Zhou JB and Sun WD. 2011. Different origins of adakites from the Dabie Mountains and the Lower Yangtze River Belt, eastern China: Geochemical constraints. *International Geology Review*, 53(5–6): 727–740
- Liu SA, Li SG, He YS and Huang F. 2010b. Geochemical contrasts between Early Cretaceous ore-bearing and ore-barren high-Mg adakites in central-eastern China: Implications for petrogenesis and Cu-Au mineralization. *Geochimica et Cosmochimica Acta*, 74(24): 7160–7178
- Liu Y, Liu HC and Li XH. 1996. Simultaneous and precise determination of 40 trace elements in rock samples using ICP-MS. *Geochimica*, 25(6): 552–558 (in Chinese with English abstract)
- Liu YS, Hu ZC, Gao S, Günther D, Xu J, Gao CG and Chen HH. 2008. In situ analysis of major and trace elements of anhydrous minerals by LA-ICP-MS without applying an internal standard. *Chemical Geology*, 257(1–2): 34–43
- Liu YS, Hu ZC, Zong KQ, Gao CG, Gao S, Xu J and Chen HL. 2010a. Reappraisal and refinement of zircon U-Pb isotope and trace

- element analyses by LA-ICP-MS. Chinese Science Bulletin, 55 (15): 1535–1546
- Liu YY, Ma CQ, Zhang C, She ZB and Zhang JY. 2009. Petrogenesis of the Yueshan pluton: Zircon U-Pb dating and Hf isotope evidence. Geological Science and Technology Information, 28(5): 22–30 (in Chinese with English abstract)
- Liu YY, Ma CQ, Lu ZY and Huang WP. 2012. Zircon U-Pb age, element and Sr-Nd-Hf isotope geochemistry of Late Mesozoic magmatism from the Guichi metallogenic district in the Middle and Lower Reaches of the Yangtze River region. Acta Petrologica Sinica, 28(10): 3287–3305 (in Chinese with English abstract)
- Ludwig KR. 2003. ISOPLOT 3.0: A geochronological toolkit for Microsoft Excel. Berkeley Geochronology Center, Special Publication, 4, 1–70
- Mao JW, Wang YT, Lehmann B, Yu JJ, Du AD, Mei YX, Li YF, Zang WS, Stein HJ and Zhou TF. 2006. Molybdenite Re-Os and albite $^{40}\text{Ar}/^{39}\text{Ar}$ dating of Cu-Au-Mo and magnetite porphyry systems in the Yangtze River valley and metallogenic implications. Ore Geology Reviews, 29(3–4): 307–324
- Mao JW, Shao YJ, Xie GQ, Zhang JD and Chen YC. 2009. Mineral deposit model for porphyry-skarn polymetallic copper deposits in Tongling ore dense district of Middle-Lower Yangtze Valley metallogenic belt. Mineral Deposits, 28(2): 109–119 (in Chinese with English abstract)
- McDonough WF and Sun SS. 1995. The composition of the Earth. Chemical Geology, 120(3–4): 223–253
- Middlemost EAK. 1985. Magmas and Magmatic Rocks. London: Longman, 1–266
- Pan YM and Dong P. 1999. The Lower Changjiang (Yangtze River) metallogenic belt, east central China: Intrusion-and wall rock-hosted Cu-Fe-Au, Mo, Zn, Pb, Ag deposits. Ore Geology Reviews, 15(4): 177–242
- Pearce JA, Harris NBW and Tindle AG. 1984. Trace element discrimination diagrams for the tectonic interpretation of granitic rocks. Journal of Petrology, 25(4): 956–983
- Peccerillo A and Taylor SR. 1976. Geochemistry of Eocene calc-alkaline volcanic-rocks from Kastamonu area, northern Turkey. Contributions to Mineralogy and Petrology, 58(1): 63–81
- Qi L, Hu J and Gregoire DC. 2000. Determination of trace elements in granites by inductively coupled plasma mass spectrometry. Talanta, 51(3): 507–513
- Soderlund U, Patchett JP, Vervoort JD and Isachsen CE. 2004. The Lu-176 decay constant determined by Lu-Hf and U-Pb isotope systematics of Precambrian mafic intrusions. Earth and Planetary Science Letters, 219(3–4): 311–324
- Song GX, Qin KZ and Li GM. 2010. Study on the fluid inclusions and S-H-O isotopic compositions of skarn-porphyry-type W-Mo deposits in Chizhou area in the Middle-Lower Yangtze Valley. Acta Petrologica Sinica, 26(9): 2768–2782 (in Chinese with English abstract)
- Sun SS and McDonough WF. 1989. Chemical and isotopic systematics of oceanic basalts; Implications for mantle composition and processes. In: Saunders AD and Norry MJ (eds.). Magmatism in Oceanic Basins. Geological Society, London, Special Publication, 42(1): 313–345
- Sun WD, Li SG, Chen YD and Li YJ. 2002. Timing of synorogenic granitoids in the South Qinling, central China: Constraints on the evolution of the Qinling-Dabie orogenic belt. Journal of Geology, 110(4): 457–468
- Sun WD, Xie Z, Chen JF, Zhang X, Chai ZF, Du AD, Zhao JS, Zhang CH and Zhou TF. 2003. Os-Os dating of copper and molybdenum deposits along the Middle and Lower Reaches of the Yangtze River, China. Economic Geology, 98(1): 175–180
- Sun WD, Arculus RJ, Kamenetsky VS and Binns RA. 2004. Release of gold-bearing fluids in convergent margin magmas prompted by magnetite crystallization. Nature, 431(7011): 975–978
- Sun WD, Ling MX, Yang XY, Fan WM, Ding X and Liang HY. 2010. Ridge subduction and porphyry copper-gold mineralization: An overview. Science China (Earth Science), 53(4): 475–484
- Sun WD, Zhang H, Ling MX, Ding X, Chuang SL, Zhou JB, Yang XY and Fan WM. 2011. The genetic association of adakites and Cu-Au ore deposits. International Geology Review, 53(5–6): 691–703
- Tang YC, Wu YC, Chu GZ, Xing FM, Wang YM, Cao FY and Chang YF. 1998. Geology of Copper-Gold Polymetallic Deposits in the along-Changjiang Area of Anhui Province. Beijing: Geological Publishing House, 1–351 (in Chinese)
- Tu YJ, Yang XY, Zheng YF and Li HM. 2001. U-Pb dating of zircon from gneiss at Nanhuang in East Anhui. Acta Petrologica Sinica, 17(1): 157–160 (in Chinese with English abstract)
- Wang Q, Wyman DA, Xu JF, Zhao ZH, Jian P, Xiong XL, Bao ZW, Li CF and Bai ZH. 2006. Petrogenesis of Cretaceous adakitic and shoshonitic igneous rocks in the Luzong area, Anhui Province (eastern China): Implications for geodynamics and Cu-Au mineralization. Lithos, 89(3–4): 424–446
- Wang Q, Wyman DA, Xu JF, Zhao ZH, Jian P and Zi F. 2007. Partial melting of thickened or delaminated lower crust in the middle of eastern China: Implications for Cu-Au mineralization. Journal of Geology, 115(2): 149–161
- Wang FY, Liu SA, Li SG, Akhtar S and He YS. 2014. Zircon U-Pb ages, Hf-O isotopes and trace elements of Mesozoic high Sr/Y porphyries from Ningzhen, eastern China: Constraints on their petrogenesis, tectonic implications and Cu mineralization. Lithos, 200–201: 299–316
- Whalen BJ, Currie KL and Chappell BW. 1987. A-type granites: Geochemical characteristics, discrimination and petrogenesis. Contributions to Mineralogy and Petrology, 95(4): 407–419
- Wong J, Sun M, Xing GF, Li XH, Zhao GC, Wong K, Yuan C, Xia XP, Li LM and Wu FY. 2009. Geochemical and zircon U-Pb and Hf isotopic study of the Baijuhuajian metaluminous A-type granite: Extension at 125–100 Ma and its tectonic significance for South China. Lithos, 112(3–4): 289–305
- Wu YB and Zheng YF. 2004. Genesis of zircon and its constraints on interpretation of U-Pb age. Chinese Science Bulletin, 49(15): 1554–1569
- Wu FY, Ji WQ, Sun DH, Yang YH and Li XH. 2012. Zircon U-Pb geochronology and Hf isotopic compositions of the Mesozoic granites in southern Anhui Province, China. Lithos, 150: 6–25
- Xie JC, Yang XY, Sun WD, Du JG, Xu W, Wu LB, Wang KY and Du XW. 2009. Geochronological and geochemical constraints on formation of the Tongling metal deposits, Middle Yangtze metallogenic belt, east-central China. International Geology Review, 51(5): 388–421
- Xie JC, Yang XY, Sun WD and Du JG. 2012. Early Cretaceous dioritic rocks in the Tongling region, eastern China: Implications for the tectonic settings. Lithos, 150: 49–61
- Xie JC, Yang XY, Xiao YL, Du JG and Sun WD. 2012. Petrogenesis of the Mesozoic intrusive rocks from the Tongling ore cluster region: The metallogenic significance. Acta Geologica Sinica, 86(3): 423–459 (in Chinese with English abstract)
- Xing FM, Xu X and Li ZC. 1994. Discovery of the Early Proterozoic basement in the Middle-Lower Reaches of Yangtze River and its significance. Chinese Science Bulletin, 39(2): 136–139
- Xue HM, Wang YG, Ma F, Wang C, Wang DE and Zuo TL. 2009. The Huangshan A-type granites with tetrad REE: Constraints on Mesozoic lithospheric thinning of the southeastern Yangtze Cratons? Acta Geologica Sinica, 83(2): 247–260 (in Chinese with English abstract)
- Yang GC, Ge LS, Lu YC, Zou YL, Xing JB, Zhang F and Yuan SS. 2014. Re-Os isotopic dating of molybdenite from the Matou iindgrenite deposit from Chizhou area in the south of Anhui Province and its geological implications. Journal of Mineralogy and Petrology, 34(1): 30–35 (in Chinese with English abstract)
- Yang SY, Jiang SY, Zhao KD, Jiang YH, Ling HF and Li L. 2012. Geochronology, geochemistry and tectonic significance of two Early Cretaceous A-type granite in the Gan-Hang Belt, Southeast China. Lithos, 150: 155–170
- Yang W and Zhang HF. 2012. Zircon geochronology and Hf isotopic

- composition of Mesozoic magmatic rocks from Chizhou, the Lower Yangtze region: Constraints on their relationship with Cu-Au mineralization. *Lithos*, 150: 37–48
- Yang XY and Lee IS. 2011. Review of the stable isotope geochemistry of Mesozoic igneous rocks and Cu-Au deposits along the Middle-Lower Yangtze Metallogenic Belt, China. *International Geology Review*, 53 (5–6): 741–757
- Yuan HL, Gao S, Liu XM, Li HM, Günther D and Wu FY. 2004. Accurate U-Pb age and trace element determinations of zircon by laser ablation-inductively coupled plasma mass spectrometry. *Geostandards and Geoanalytical Research*, 28(3): 353–370
- Yuan HL, Gao S, Dai MN, Zong CL, Günther D, Fontaine GH, Liu XM and Diwu CR. 2008. Simultaneous determinations of U-Pb age, Hf isotopes and trace element compositions of zircon by excimer laser-ablation quadrupole and multiple-collector ICP-MS. *Chemical Geology*, 247(1–2): 100–118
- Zhai YS, Yao SZ, Lin XD, Zhou XR, Wan TF, Jin FQ and Zhou ZG. 1992. Metallogeny of Iron and Copper Deposits in the Middle-Lower Yangtze River Region. Beijing: Geological Publishing House, 1–194 (in Chinese)
- Zhang S, Zhang ZC, Ai Y, Yuan WM and Ma LT. 2009. The petrology, mineralogy and geochemistry study of the Huangshan granite intrusion in Anhui Province. *Acta Petrologica Sinica*, 25(1): 25–38 (in Chinese with English abstract)
- Zhang ZY, Du YS, Zhang J and Pang ZS. 2011. SHRIMP Zircon U-Pb geochronology, petrochemical and geochemical characteristics of Tongshan intrusion in Guichi, Anhui Province. *Geological Review*, 57(3): 366–378 (in Chinese with English abstract)
- Zheng YF, Zhao ZF, Wu YB, Zhang SB, Liu X and Wu FY. 2006. Zircon U-Pb age, Hf and O isotope constraints on protolith origin of ultrahigh-pressure eclogite and gneiss in the Dabie orogen. *Chemical Geology*, 231(1–2): 135–158
- Zhu ZY, Jiang SY, Hu J, Gu LX and Li JW. 2014. Geochronology, geochemistry, and mineralization of the granodiorite porphyry hosting the Matou Cu-Mo (\pm W) deposit, Lower Yangtze River metallogenic belt, eastern China. *Journal of Asian Earth Sciences*, 79(B): 623–640
- Zhou TF, Fan Y and Yuan F. 2008. Advances on petrogenesis and metallogeny study of the mineralization belt of the Middle and Lower Reaches of the Yangtze River area. *Acta Petrologica Sinica*, 24(8): 1665–1678 (in Chinese with English abstract)
- Zhou TF, Fan Y and Yuan F. 2012. Progress of geological study in the Middle-lower Yangtze River valley metallogenic belt. *Acta Petrologica Sinica*, 28(10): 3051–3066 (in Chinese with English abstract)
- 附中文参考文献**
- 常印佛, 刘湘培, 吴言昌. 1991. 长江中下游铜铁成矿带. 北京: 地质出版社, 294–312
- 董胜. 2006. 安徽省贵池地区区域地球化学特征及找矿意义. 物探与化探, 30(3): 215–223
- 段留安, 杨晓勇, 汪方跃, 邓江洪, 孙卫东. 2012. 长江中下游成矿带贵池抛刀岭金矿含矿岩体年代学及地球化学研究. 岩石学报, 28(10): 3241–3254
- 段留安, 杨晓勇, 刘晓明, 孙卫东. 2013. 铜陵舒家店地区志留纪地层中金矿的发现及其意义. 大地构造与成矿学, 37(2): 333–339
- 段留安, 杨晓勇, 汪方跃. 2014. 长江中下游成矿带抛刀岭大型斑岩型金矿特征及找矿前景. 地球科学与环境学报, 36(1): 161–170
- 范裕, 周涛发, 袁峰, 钱存超, 陆三明, Cooke D. 2008. 安徽庐江-枞阳地区 A 型花岗岩的 LA-ICP-MS 定年及其地质意义. 岩石学报, 24(8): 1715–1724
- 李献华, 赵振华, 桂训唐, 于津生. 1991. 华南前寒武纪地壳形成时代的 Sm-Nd 和锆石 U-Pb 同位素制约. 地球化学, 20(3): 255–264
- 刘颖, 刘海臣, 李献华. 1996. 用 ICP-MS 准确测定岩石样品中的 40 余种微量元素. 地球化学, 25(6): 552–558
- 刘园园, 马昌前, 张超, 余振兵, 张金阳. 2009. 安徽月山闪长岩的成因探讨——锆石 U-Pb 定年及 Hf 同位素证据. 地质科技情报, 28(5): 22–30
- 刘圆圆, 马昌前, 吕昭英, 黄卫平. 2012. 长江中下游贵池矿集区燕山期岩浆作用及其地质意义: 年代学、地球化学及 Sr-Nd-Hf 同位素证据. 岩石学报, 28(10): 3287–3305
- 毛景文, 邵拥军, 谢桂青, 张建东, 陈毓川. 2009. 长江中下游成矿带铜陵矿集区铜多金属矿床模型. 矿床地质, 28(2): 109–119
- 宋国学, 秦克章, 李光明. 2010. 长江中下游池州地区矽卡岩-斑岩型 W-Mo 矿床流体包裹体与 H、O、S 同位素研究. 岩石学报, 26(9): 2768–2782
- 唐永成, 吴言昌, 储国正, 邢凤鸣, 王永敏, 曹奋扬, 常印佛. 1998. 安徽沿江地区铜金多金属矿床地质. 北京: 地质出版社, 1–351
- 涂荫玖, 杨晓勇, 郑永飞, 李惠民. 2001. 皖东南黄片麻岩的锆石 U-Pb 年龄. 岩石学报, 17(1): 157–160
- 吴元保, 郑永飞. 2004. 锆石成因矿物学研究及其对 U-Pb 年龄解释的制约. 科学通报, 49(16): 1589–1604
- 谢建成, 杨晓勇, 肖益林, 杜建国, 孙卫东. 2012. 铜陵矿集区中生代侵入岩成因及成矿意义. 地质学报, 86(3): 423–459
- 薛怀民, 汪应庚, 马芳, 汪诚, 王德恩, 左廷龙. 2009. 高度演化的黄山 A 型花岗岩: 对扬子克拉通东南部中生代岩石圈减薄的约束? 地质学报, 83(2): 247–260
- 杨贵才, 葛良胜, 路英川, 邹依林, 邢俊兵, 张峰, 袁士松. 2014. 安徽省池州地区马头钼矿辉钼矿 Re-Os 年龄及其地质意义. 矿物岩石, 34(1): 30–35
- 翟裕生, 姚书振, 林新多, 周珣若, 万天丰, 金福全, 周宗桂. 1992. 长江中下游地区铁铜(金) 成矿规律. 北京: 地质出版社, 1–194
- 张舒, 张招崇, 艾羽, 袁万明, 马乐天. 2009. 安徽黄山花岗岩岩石学、矿物学及地球化学研究. 岩石学报, 25(1): 25–38
- 张智宇, 杜杨松, 张静, 庞振山. 2011. 安徽贵池铜山岩体 SHRIMP 锆石 U-Pb 年代学与岩石地球化学特征研究. 地质论评, 57(3): 366–378
- 周涛发, 范裕, 袁峰. 2008. 长江中下游成矿带成岩成矿作用研究进展. 岩石学报, 24(8): 1665–1678
- 周涛发, 范裕, 袁峰. 2012. 长江中下游成矿带地质与矿产研究进展. 岩石学报, 28(10): 3051–3066